

1 **Measurement Report: Rapid decline of aerosol absorption**
2 **coefficient and aerosol optical properties effects on radiative**
3 **forcing in an urban areasarea of Beijing from 2018 to 2021**

4 Xinyao Hu^{1,2}, Junying Sun^{1,3*}, Can Xia^{1,4}, Xiaojing Shen¹, Yangmei Zhang¹, Quan Liu¹,
5 Zhaodong Liu^{1,4}, Sinan Zhang¹, Jialing Wang¹, Aoyuan Yu^{1,2}, Jiayuan Lu¹, Shuo Liu¹, and
6 Xiaoye Zhang¹

7 ¹State Key Laboratory of Severe Weather & Key Laboratory of Atmospheric Chemistry of
8 CMA, Chinese Academy of Meteorological Sciences, Beijing 100081, China

9 ²University of Chinese Academy of Sciences, Beijing 100049, China

10 ³State Key Laboratory of Cryospheric Science, Northwest Institute of Eco-Environment
11 and Resources, Chinese Academy of Sciences, Lanzhou 730000, China

12 ⁴Nanjing University of Information Science & Technology, Nanjing 210044, China

13 *Correspondence to: Junying Sun (jysun@cma.gov.cn)

14 **Abstract**

15 Reliable observations of aerosol optical properties are crucial for quantifying the
16 radiative forcing of climate. The simultaneous measurements of aerosol optical properties
17 at three wavelengths for PM₁ and PM₁₀ were conducted in urban Beijing from March 2018
18 to February 2022. ~~The results showed considerable reductions in~~The aerosol absorption
19 coefficient (σ_{ab}) at 550 nm of PM₁₀ and PM₁ decreased by 55.0% and 53.5% from 2018 to
20 2021. Significant reduction in σ_{ab} may be related to reduced primary emissions caused by

21 effective air pollution control measures. PM_{2.5} mass concentration decreased by 34.4%
22 from 2018 to 2021. SSA increased from 0.89 ± 0.04 for PM₁₀ (0.87 ± 0.05 for PM₁) in 2018
23 to 0.93 ± 0.03 for PM₁₀ (0.91 ± 0.04 for PM₁) in 2021. ~~These results indicated~~ Increasing
24 SSA and decreasing PM_{2.5} mass concentration suggest that the fraction of absorbing
25 aerosols ~~were more effectively controlled than scattering aerosols~~ decreased with improved
26 air quality due to pollution control measure-taking. The annual average submicron
27 absorption ratio (R_{ab}) increased from 86.1% in 2018 to 89.2% in 2021, suggesting that fine
28 particles are the main contributors to total PM₁₀ absorption and that the fine particles to
29 absorption became more important. Absorption Angstrom exponent (AAE) in winter
30 decreased from 2018 to 2021, implying a decreasing contribution from brown carbon to
31 light absorption, which may relate to the ~~decreased~~ reduced emissions of biomass burning
32 and coal combustion. During the study period, aerosol radiative forcing efficiency became
33 more negative mainly influenced by increasing SSA, and ~~were~~ was -27.0 and -26.2 W m^{-2}
34 AOD^{-1} for PM₁₀ and PM₁ in 2021, ~~which was mainly influenced by increasing SSA.~~
35 Higher σ_{ab} and PM_{2.5} mass concentrations were ~~mainly~~ primarily distributed in clusters 4
36 and 5, transported from the south and the west of Beijing ~~in~~ each year. σ_{ab} and PM_{2.5}
37 corresponding to clusters 4 and 5 decreased evidently from 2018 to 2021, which may result
38 from the control of source emissions in surrounding regions of Beijing. The 4-year data
39 presented in this study provide critical optical parameters for radiative forcing assessment
40 within two size ranges and are helpful for evaluating the effectiveness of clean air action.

41 **1 Introduction**

42 Atmospheric aerosols perturb the Earth's atmospheric radiation balance and climate
43 forcing by directly affecting the scattering and absorption of solar radiation (Charlson et
44 al., 1992; Jacobson, 2001) but also indirectly affecting cloud reflectivity and precipitation
45 processes (Twomey, 2007). Light-scattering aerosols contribute to offsetting the warming
46 effect of CO₂, while absorbing aerosols contribute to the heating of the atmosphere (Bond
47 and Bergstrom, 2007), and produce a positive radiative forcing (Segura et al., 2016). The
48 largest contribution to aerosol absorption is from black carbon (BC), which absorbs
49 strongly over the entire solar spectrum (Bond and Bergstrom, 2007). Dust and brown
50 carbon (BrC) are also light absorption aerosols, which strongly absorb in the ultraviolet
51 (UV) spectrum. Globally, aerosols contributed an effective radiative forcing (ERF) of -1.3
52 $\pm 0.7 \text{ W m}^{-2}$, and the ERF due to emissions of BC is now estimated to be 0.11 (-0.20 to
53 0.42) W/m^2 between 1750 to 2019 (Szopa et al., 2021). However, aerosol properties are
54 highly spatial and temporal variationvariable, which results in radiative forcing variation
55 from local to global scales and creates an observational challenge (Collaud Coen et al.,
56 2013; Ealo et al., 2018; Andrews et al., 2011). Therefore, reliable observations of aerosol
57 optical properties are crucial for quantifying the radiative forcing of climate.

58 In order to assess the role of aerosols on climate forcing accurately, a set of parameters
59 that describe aerosol's optical properties are needed, such as scattering coefficient (σ_{sp}),
60 absorption coefficient(σ_{ab}), backscatter fraction(b) and single scattering albedo (SSA). SSA
61 is a key variable that determines the magnitude and the sign of the aerosol forcing (J.
62 Hansen et al., 1997; Lee et al., 2007; Li et al., 2022a; Zhang et al., 2020). Previous

63 ~~studies~~ found that ~~typical SSA~~ values ~~of SSA are between~~ range from slightly less than
64 0.8 ~~and to almost purely scattering particles with SSA close to~~ 1 at worldwide locations
65 (Laj et al., 2020; Pandolfi et al., 2018), ~~with~~ higher SSA values ~~indicating~~ indicate a
66 tendency towards a cooling effect (Li et al., 2022a). The backscatter fraction (b) describes
67 how much aerosol particles scatter radiation in the backward hemisphere compared with
68 the total scattering, which is a crucial variable for aerosol radiative forcing efficiency (RFE)
69 calculations (Andrews et al., 2011; Sheridan and Ogren, 1999; Luoma et al., 2019).
70 Previous studies found that the magnitude of RFE increases with increasing b (Shen et al.,
71 2018). Typical values of b for the atmospheric aerosol at 550 nm were from approximately
72 0.05 to 0.20 (Titos et al., 2021).

73 Besides, aerosol optical properties are wavelength-dependent, absorption Angstrom
74 exponent (AAE) describes the spectral dependence of light absorption by aerosols and is
75 typically used to differentiate between different aerosol types (Helin et al., 2021). The AAE
76 for fresh BC is ~ 1 , indicating “weak” spectral dependence of light absorption (Bond et al.,
77 2013; Bond and Bergstrom, 2007), and the AAE > 1 indicates the presence of BrC or dust,
78 which tend to exhibit absorption that increases sharply as wavelength decreases
79 (Moosmüller et al., 2009; Lack and Cappa, 2010). Thus, obtaining the aerosol absorption
80 coefficient at different wavelengths is essential and can be helpful to differentiate between
81 different aerosol types.

82 As one of the world’s most populous and rapidly developing megacities, Beijing
83 experienced rapid economic growth and urbanization, accompanied by severe air pollution.
84 Many in-situ measurements of aerosol optical properties have been conducted in Beijing
85 (Bergin et al., 2001; He et al., 2009; Garland et al., 2009; Jing et al., 2015; Wang et al.,

86 2019; Zhao et al., 2019; Xia et al., 2020). Previous studies found that high aerosol loading
87 leads to large σ_{ab} in Beijing (Jing et al., 2015; Garland et al., 2009; Bergin et al., 2001).
88 Moreover, the AAE showed significant seasonal variations in Beijing. Significantly higher
89 AAE in winter than in summer highlights the important role of absorption of non-BC
90 components (e.g. BrC) in winter (Xie et al., 2020; Xia et al., 2020). In order to reduce
91 emissions and improve air quality, the government implemented strict pollution control
92 measures (Xu and Zhang, 2020). Significant decreases in $PM_{2.5}$ mass concentrations were
93 found in Beijing and the annual mean elemental carbon (EC) concentrations declined from
94 4.0 to 2.6 $\mu g m^{-3}$ from March 2013 to February 2018 in Beijing (Ji et al., 2019). Xia et al.
95 (2020) separated and quantified the effects of emission control and meteorological
96 transport variability on BC loading from 2015 to 2017 in north China Plain. However, the
97 environmental effects caused by emission controls are related to not only their mass
98 concentrations, but also their optical properties and radiative effect (Luo et al., 2020).
99 Therefore, it's necessary to investigate the multiple-year variations in aerosol optical
100 properties and radiative effect in providing a comprehensive understanding of the effects
101 of emission control. Wang et al. (2019) found that absorption coefficient (σ_{ap}) for $PM_{2.5}$
102 decreased from 2014 to 2017, with a significant decrease of σ_{ap} in autumn. Sun et al. (2022)
103 estimated that the direct radiative forcing of BC decreased by 67% from $+3.36 W m^{-2}$ in
104 2012 to $+1.09 W m^{-2}$ in 2020. However, these studies were mostly conducted with
105 conventional total suspended particulate (TSP) cyclone, $PM_{2.5}$ size cut, or PM_{10} size cut.
106 Few studies focused on the sub-micron and super-micron particle optical properties and
107 estimated aerosol radiative effect in the post-“Action Plan on Prevention and Control of
108 Air Pollution” era. Acquiring the aerosol optical for the total ($< 10\mu m$ diameter) and

109 submicron aerosol is also in line with the aerosol advisory group of the Global Atmosphere
110 Watch recommendation (WMO/GAW, 2016).

111 In this study, the simultaneous measurements of aerosol optical properties at three
112 wavelengths for PM₁ and PM₁₀ were conducted in urban Beijing from March 2018 to
113 February 2022. The annual, seasonal, and diurnal variations of aerosol optical properties
114 for two size cuts were investigated. The scattering properties of aerosols for two size ranges
115 (PM₁₀ and PM₁) under dry conditions observed in Beijing have been analyzed in detail by
116 Hu et al. (2021). Thus, this study mainly focused on the variation of aerosol absorption
117 coefficient, single scattering albedo, and absorption Angstrom Exponent for PM₁₀ and PM₁.
118 Moreover, the aerosol radiative effects in two size cuts were estimated. Finally, the
119 transport and its impact on aerosol optical properties were analyzed. The 4-year data
120 presented in this study provide key optical parameters for radiative forcing assessment
121 within two size ranges and are helpful for evaluating the effectiveness of clean air action.

122 **2 Instrumentation and methods**

123 **2.1 Site description**

124 The sampling site in this study is located on the roof of the Chinese Academy of
125 Meteorological Sciences (CAMS, 116°19' E, 39°57' N, 46 m a.s.l) in Beijing, which is a
126 typical urban site in the northwest of Beijing between the 2nd and 3rd ring roads. The
127 laboratory is approximately on the roof of CAMS building, and the measurements are taken
128 at 53 m above ground level. The site is mainly influenced by local emissions from
129 residential living and traffic pollution (Xia et al., 2019).

2.2 Aerosol absorption Instruments and measurements

The ambient air was sampled into a PM₁₀ impactor with 16.7 LPM and then to an adsorption aerosol dryer, which controlled the relative humidity (RH) of sample air below 30% (Tuch et al., 2009). The dried aerosol sample passes through switched impactors that toggle the aerosol size cut between 1.0 μm (<1 μm) and 10 μm (<10 μm) aerodynamic particle diameters every 30 min, thus allowing to measure both fine and coarse particles (Hu et al., 2021). The sample aerosol was then passed into the Nephelometer (TSI Inc., Model 3563) and Tricolor Absorption Photometer (TAP, Brechtel Manufacturing, Inc., Hayward, CA, USA).

The integrating nephelometer measured the scattering coefficient (σ_{sp}) (angular range of 7–170°) and backscattering coefficient (σ_{bsp}) (angular range of 90–170°) at 450, 550, and 700 nm. The scattering and backscattering coefficient were corrected for truncation and instrument non-idealities using the method described by Anderson and Ogren (1998). Details are given in Hu et al. (2021). To ensure the data's accuracy and reliability, the nephelometer was calibrated regularly using filtered ambient air using a HEPA filter and CO₂ with a purity of 99.999%. A zero-check was automatically performed once per hour to obtain a nephelometer background.

TAP measures absorption coefficient (σ_{ab}) at 465, 520, and 640 nm with the 47 mm diameter, glass-fiber filter and is a commercially available version of the continuous light absorption photometer (CLAP), which is low cost and high sensitivity (Ogren et al., 2017). The TAP comprises eight sample spots and two reference spots. The aerosol-laden air passes through one sample spot at a time, which allows for 8 times the filter lifetime compared to single-spot photometers (Davies et al., 2019). Unlike the Multi-Angle

153 Absorption Photometer (MAAP), TAP does require a co-located aerosol light scattering or
 154 extinction measurement to derive aerosol light absorption (Ogren et al., 2017). Thus,
 155 simultaneous observation of aerosol light scattering has been measured and used to correct
 156 absorption data. When the Nephelometer and TAP were calibrated or malfunctioning, no
 157 data are available. During this study, 84% of the data was effective.

158 **2.3. Data processing**

159 The TAP measures the light transmitted through a filter as particles are deposited onto
 160 the filter. The filter attenuation coefficient (σ_{atn}), at a specific wavelength (λ), can be
 161 determined as:

$$162 \quad \sigma_{atn}(\lambda) = \frac{A}{Q} \times \frac{\Delta atn(\lambda)}{\Delta t} \quad (1)$$

163 where $\Delta atn(\lambda)$ is the filter attenuation at times t_1 and t_2 , A is the area of on the filter,
 164 and Q is the sample flow rate through the filter.

165 In order to correct the error caused by multiple scattering and filter loading, the aerosol
 166 light absorption coefficient ($\sigma_{ab}(\lambda)$) was corrected based on the methods of Bond et al.
 167 (1999) and Ogren et al. (2017). First, the effect of filter loading was calibrated based on
 168 Eq. (2):

$$169 \quad \sigma_{ab}(\lambda)_{raw} = \frac{0.85 \times \sigma_{atn}(\lambda)}{K_2 \times (1.0796 \times Tr(\lambda) + 0.71)} \quad (2)$$

170 Then, $\sigma_{ab}(\lambda)_{raw}$ at 465, 520, and 640 nm were adjusted to the wavelength of the
 171 light scattering coefficient based on the calculated AAE. Finally, the multiple scattering
 172 effect was corrected based on Eq. (3):

$$173 \quad \sigma_{ab}(\lambda) = \sigma_{ab}(\lambda)_{raw} - \frac{K_1 \times \sigma_{sp}(\lambda)}{K_2} \quad (3)$$

174 where $Tr(\lambda)$ is the normalized filter transmittance at time t relative to transmittance
175 at the start of sampling ($t=0$) and σ_{sp} is the aerosol light-scattering coefficient at 450, 550,
176 and 700 nm measured by the nephelometer. K_1 and K_2 were derived by Bond et al. (1999)
177 as $K_1 = 0.02 \pm 0.02$ and $K_2 = 1.22 \pm 0.20$, where the uncertainties are given for the 95%
178 confidence level.

179 Using the corrected absorption coefficient data, the following parameters were
180 calculated:

181 Absorption Angstrom exponent (AAE) describes the spectral dependence of light
182 absorption.

$$183 \quad AAE = -\frac{\ln(\sigma_{ab}^{\lambda_1}/\sigma_{ab}^{\lambda_2})}{\ln(\lambda_1/\lambda_2)} \quad (4)$$

184 The submicron absorption ratio (Rab) is determined as the ratio of the absorption
185 coefficients for PM_{10} and PM_{10} .

$$186 \quad Rab = \frac{\sigma_{ab}(D < 1 \mu m)}{\sigma_{ab}(D < 10 \mu m)} \quad (5)$$

187 where $\sigma_{ab}(D < 1 \mu m)$ and $\sigma_{ab}(D < 10 \mu m)$ are σ_{ab} for particle diameters $< 1 \mu m$ and 10
188 μm , respectively.

189 Aerosol radiative forcing efficiency (RFE) at top-of-the-atmosphere (TOA) is a
190 simplified formula that describes how large of an impact the aerosols would make to the
191 aerosol radiative forcing (ΔF) per unit of aerosol optical depth (AOD) (Sheridan and Ogren,
192 1999) and we estimated the RFE at TOA as the Eq.6 (Haywood and Shine, 1995; Sheridan
193 and Ogren, 1999):

194
$$\text{RFE} = \frac{\Delta F}{\text{AOD}} = -DS_0 T_{\text{at}}^2 (1 - A_C) \times \text{SSA} \times \beta \times ((1 -$$

 195
$$R_s)^2 - (\frac{2R_s}{\beta}) \times (\frac{1}{\text{SSA}} - 1)) \quad \text{---(6)}$$

196 where D is the fractional day length, S₀ is the solar constant, T_{at} is the atmospheric
 197 transmission, A_c is the fractional cloud amount, and R_s is the surface reflectance. The
 198 constants used were D = 0.5, S₀ = 1370 Wm⁻², T_{at} = 0.76, A_c = 0.6, and R_s = 0.15 as
 199 suggested by Haywood and Shine (1995), and upper scatter fraction β was calculated from
 200 $\beta = 0.0817 + 1.8495 \times b - 2.9682 \times b^2$. backscatter ~~ratio~~fraction (b) was calculated based on
 201 scattering coefficient (σ_{sp}) and backscattering coefficient (σ_{bsp}) measured by Nephelometer
 202 as $b = \sigma_{\text{bsp}} / \sigma_{\text{sp}}$. Equation (6) has been widely used to assess the intrinsic radiative forcing
 203 efficiency of aerosols at the top of the atmosphere (Sheridan and Ogren, 1999; Virkkula et
 204 al., 2011; Shen et al., 2018). Note that RFE in this study was in a dry condition. As the
 205 backscatter fraction and single scattering albedo are all RH-dependent, the RFE is also
 206 sensitive to RH (Fierz-Schmidhauser et al., 2010). Previous studies revealed that RFE
 207 increased as the elevating RH (Titos et al., 2021; Xia et al., 2023). In this study, the values
 208 of ΔF at TOA were also calculated by multiplying the RFE for PM₁₀ with the AOD of
 209 ambient atmospheric aerosols observed at the CAMS site during the study periods. AOD
 210 can be downloaded from Aerosol Robotic Network (AERONET). Note that RFE was at a
 211 dry state, thus the ΔF at TOA here may be slightly underestimated.

212 **2.4. Other data used**

213 The hourly PM_{2.5} and PM₁₀ mass concentrations were measured at Guan yuan station,
 214 which is about 3km from the CAMS site. The data can be derived from the national air
 215 quality real-time publishing platform (<http://106.37.208.233:20035/>). The hourly

216 meteorological data were measured at Haidian station (station No. 54399) and obtained
217 from the National Meteorological Information Center of China Meteorological
218 Administration.

219 **2.5. Back trajectories analysis**

220 To investigate the influence of air mass origins on aerosol optical properties, 48-h
221 backward trajectories arriving at Beijing at a height of 500 m above ground level were
222 calculated from 0:00 to 23:00 local time each day from March 2018 to February 2022,
223 using the Trajstat Software, combined with HYSPLIT 4 model (Hybrid Single-Particle
224 Lagrangian Integrated Trajectory), and the NCEP Global Data Assimilation System
225 (GDAS) data with a $1^\circ \times 1^\circ$ resolution (Draxler and Hess, 1998; Wang et al., 2009).

226 In this study, four seasons are defined as follows: spring from March to May, summer
227 from June to August, autumn from September to November, and winter from December to
228 the following February, and all data are reported in Beijing time (UTC+8).

229 **3 Results and discussion**

230 **3.1 Temporal variation of aerosol optical properties**

231 Figure 1 shows the annual variation of σ_{ab} , SSA, Rab, and PM_{2.5} mass concentration
232 from 2018 to 2021. During the study period, the annual mean PM_{2.5} in 2018 was 54.7 μg
233 m^{-3} , and it decreased by 34.4% (35.9 $\mu\text{g} \text{m}^{-3}$) in 2021, which suggested that the strict
234 pollution control measures are effective in reducing the PM loadings in Beijing (Lei et al.,
235 2021). Gong et al. (2022) demonstrated that emission reduction dominated the variations
236 of PM_{2.5} mass concentration in Beijing from 2013 to 2020, and meteorology and emission

237 reduction contributed 7% and 63.2% of decreases, respectively. σ_{ab} at 550 nm of PM₁₀ and
238 PM₁ showed similar annual variations. The annual mean σ_{ab} at 550 nm of PM₁₀ and PM₁
239 decreased by 55.0% and 53.5%, respectively. ~~A significant decrease in σ_{ab} indicated the~~
240 ~~effective control of absorbing aerosols, which was mainly related to decreasing biomass~~
241 ~~burning and coal consumption, increasing usage of natural gases, and the implementation~~
242 ~~of a stricter vehicular emission standard in recent years (Sun et al., 2022).~~, from 2018 to
243 2021. The Mann–Kendall trend test supported that the decrease in σ_{ab} for PM₁ and PM₁₀
244 from 2018 to 2021 was significant (Table S1). Carbonaceous aerosol, especially black
245 carbon, is closely related to aerosol absorption (Yang et al., 2009). A continuous decrease
246 in σ_{ab} was consistent with the continuous reduction of black carbon concentration observed
247 in Beijing in previous studies (Ji et al., 2019; Sun et al., 2022), which was mainly related
248 to significantly reduced primary emissions caused by effective air pollution control
249 measures in recent years (Xia et al., 2020). The annual mean σ_{ab} for PM₁₀ and PM₁ in 2021
250 was 9.8 Mm⁻¹ and 8.7 Mm⁻¹, which were both lower than the result observed in Nainital,
251 in the GH region, India (Dumka et al., 2015), ~~but both higher than SMEAR II station~~
252 ~~located in Hyytiälä, southern Finland (Luoma et al., 2019).~~ and the measurement at an
253 urban site in Spain from March 2006 to February 2007 (Titos et al., 2012). In fact, with the
254 emission reduction and improvement of air quality, the aerosol scattering coefficient (σ_{sp})
255 for PM₁₀ and PM₁ also decreased in Beijing. Hu et al. (2021) revealed that σ_{sp} decreased
256 by approximately 18.4% for PM₁₀, and 16.7% for PM₁ from 2018 to 2019 in Beijing.
257 Atmospheric conditions also have an effect on aerosol optical properties. The variations of
258 meteorological parameters from 2018 to 2021 (Figure S4) showed that pressure, wind
259 speed, temperature, and RH varied slightly, while accumulated precipitation increased in

260 2021 compared with the other 3 years. On the other hand, a correlation analysis was made
261 between aerosol optical properties and meteorological parameters. The Pearson correlation
262 coefficients (R) between σ_{ab} and meteorological parameters (Table S2) are lower than 0.5,
263 indicating that a weak correlation ($R < 0.5$) was found between σ_{ab} and meteorological
264 parameters. This suggests that the meteorological parameters' influence on σ_{ab} is minor.
265 Xia et al. (2020) revealed that the effect of emission reduction was the major reason for the
266 decrease of BC in Beijing. Actually, σ_{ab} that was observed at a background station in China
267 and the European stations, which was with time series longer than 10 years, also observed
268 the reduction. σ_{ab} showed a statistically significant decreasing trend in Mt. Waliguan, a
269 background station in China, from 2008–2018 (Collaud Coen et al., 2020), which was
270 similar to a decreasing trend of black carbon (BC) in Mt. Waliguan from 2008-2017, mainly
271 related to emission reduction (Dai et al., 2021). A statistically significant decrease of 10-
272 year σ_{ap} was found in 12 stations in Europe, which was similar to a decreasing trend in BC
273 concentration in Europe related primarily to traffic emission decreases (Collaud Coen et
274 al., 2020).

275 SSA is a key variable in assessing the aerosol radiative forcing. The variation of SSA
276 also reflects the the ratio of aerosol scattering to total extinction with aerosol composition
277 changes. The annual variations of SSA for PM_{10} and PM_1 were similar. During 2018-2021,
278 annual mean SSA at 550 nm increased from 0.89 ± 0.04 for PM_{10} (0.87 ± 0.05 for PM_1) in
279 2018 to 0.93 ± 0.03 for PM_{10} (0.91 ± 0.04 for PM_1) in 2021, ~~which demonstrated that the~~
280 ~~absorbing aerosols were effectively controlled compared to scattering aerosols during the~~
281 ~~past four years. On the other hand, increasing SSA also implied that scattering aerosols~~
282 ~~play a more important role in radiative forcing in urban Beijing.~~ Increasing SSA and

283 decreasing PM_{2.5} mass concentration during the past four years suggested that the fraction
284 of absorbing aerosols became lower compared to scattering aerosols with the improvement
285 of air quality due to pollution control measure-taking. Collaud Coen et al. (2020) found
286 that SSA observed in Mt. Waliguan, a background station in Asia, presented an increasing
287 trend based on 10-year datasets, which were related to more recent abatement policies. The
288 mean submicron absorption ratio (R_{ab}) increased yearly during the same period. It was
289 from 86.1% in 2018 to 89.2% in 2021, suggesting that fine particles are the main
290 contributors to total PM₁₀ absorption, and the contributions from fine particles to
291 absorption became more important.

292 The σ_{ab} , SSA, and AAE for PM₁ and PM₁₀ showed similar annual variations in all
293 seasons (Fig. 2 and Fig. S1). Thus, if not stated otherwise, the following discussion takes
294 the aerosol optical properties of PM₁₀ as an example. As shown in Fig. 2 seasonal average
295 of σ_{ab} presented a decreasing trendcontinuous reduction during all seasons from 2018 to
296 2021, reflecting the reduction of absorbing aerosols which were related to effective control
297 of absorbing aerosols emissions in Beijing. σ_{ab} decreased by half in autumn and winter
298 during the study period, which was probably due to reducing coal consumption as a heating
299 source and the reduction of biomass burning. Compared with 2018, σ_{ab} in the winter of
300 2019, 2020 and 2021 decreased by 3.0%, 24.9% and 53.2%, respectively. In the winter of
301 2019, the lockdown of COVID-19 caused emission reduction from human activities in
302 China (Le et al., 2020; Tian et al., 2020), however, the unexpected smallest reduction of
303 σ_{ab} was observed in the winter of 2019 compared with the winter of 2020 and 2021. This
304 is related to the fact that severe haze pollution still occurred in the North China Plain and
305 BC concentrations rose unexpectedly during the lockdown period (Liu et al., 2021; Jia et

306 [al., 2021](#)). In particular, σ_{ab} for PM_1 and PM_{10} decreased even up to 63% and 67% in the
307 summer from 2018 to 2021. Traffic is a relatively stable source of absorption aerosols in
308 summer (Li et al., 2022b). The largest deduction of σ_{ab} was in summer and could be related
309 to more strict vehicle emission standards (Zhang et al., 2019).

310 In general, AAE was lowest in summer and highest in winter. The mean values of
311 AAE for PM_{10} were 1.13 and 1.41 in summer and winter, respectively, similar to result at
312 an urban site in Beijing in 2018 (Xie et al., 2020). During summer, the average AAE was
313 generally close to 1, which suggested that BC from traffic emissions was the major
314 component of light-absorbing aerosols. Li et al. (2022b) found that the percentage of liquid
315 fuel (traffic) contributing to the total BC was 86.8% in summer in Beijing. The highest
316 AAE suggested that BrC contributed to light absorption strongest in winter, which is due
317 to enhanced emissions from biomass burning and coal combustion in winter (Sun et al.,
318 2018). Notably, AAE decreased in winter from 1.48 for PM_{10} (1.48 for PM_1) in 2018 to
319 1.37 for PM_{10} (1.34 for PM_1) in 2021 (Fig. 2 and Fig. S1), indicating a decreasing
320 contribution from BrC to light absorption, which may relate to the effect control of biomass
321 burning and coal combustion caused by changes in heating energy structure (Ji et al., 2022).
322 To improve air quality, the Beijing-Tianjin-Hebei region adjusted the energy structure
323 during the heating period and developed clean heating projects, such as the “coal to gas”
324 project (Zhao et al., 2020; Liu et al., 2019). During the whole period, AAE was similar in
325 spring and autumn indicating that light-absorbing aerosols were from similar emission
326 sources in spring and autumn (Ran et al., 2016). AAE slightly increased in spring and
327 autumn from 2018 to 2021. Part of the reason was the occurrence of multiple fugitive dust
328 in spring and autumn (Yi et al., 2021; Gui et al., 2022). On the other hand, BrC could also

329 be formed from secondary reactions (Bond et al., 2013; Wang et al., 2022). A slight
330 increase in AAE in spring and autumn may also have been caused by a greater amount of
331 secondary organic aerosol formation as a result of an increased atmospheric oxidation
332 capacity (Ji et al., 2019; Lei et al., 2021).

333 The seasonal mean SSA ~~showed an increasing trend~~increased in all seasons from 2018
334 to 2021, indicating that the contribution of scattering aerosols to extinction increased. This
335 suggested that more effective control of scattering aerosols should be attached more
336 importance in order to improve visibility in the future. In particular, SSA in winter
337 increased significantly from 0.88 in 2018 to 0.93 in 2021, which revealed that the
338 proportion of absorbing aerosols decreases considerably in winter. This is consistent with
339 recent research which suggests that air pollution control measures has been more effective
340 in reducing the primary pollution emissions than secondary species (Vu et al., 2019; Sun
341 et al., 2020). On the other hand, seasonal mean SSA for PM₁₀ was 0.94±0.04, 0.94±0.04,
342 0.92± 0.04, 0.93±0.03 in spring, summer, autumn, and winter 2021. Similar SSA suggests
343 that the proportions of light absorbing and scattering components became relatively stable
344 in four seasons.

345 Figure 3 shows the diurnal variations of σ_{ab} and SSA at 550 nm for PM₁₀, which are
346 similar to those for PM₁ (Figure. S2). In the past four years, σ_{ab} was lower during the day
347 and higher at night in four seasons. This was consistent with that observed at an urban site
348 in Beijing during 2014-2016 (Wang et al., 2019). The evolution of the planetary boundary
349 layer had an important influence on the diurnal variation of the σ_{ab} . With stronger solar
350 radiation, the boundary layer was more fully developed during the daytime, and after sunset,
351 the convective boundary layer underwent a transition to the nocturnal stable boundary layer

352 (Guo et al., 2016). Furthermore, emissions also affected the diurnal variation of the σ_{ab} . For
353 example, heavy-duty diesel trucks and heavy-duty vehicles were only allowed to enter
354 urban areas from 23:00 to the following day 06:00 (Hu et al., 2021). As a response, the
355 minimum σ_{ab} occurred during 12:00–18:00, when the planetary boundary layer was well-
356 developed, and truck emission was lower. With shallow boundary layer height and
357 enhanced emissions from heavy-duty trucks, σ_{ab} reached the maximum at night. During the
358 study period, SSA showed a significant peak in the afternoon in four seasons, which was
359 similar to previous studies in urban Beijing (Zhao et al., 2019; Wang et al., 2019). Higher
360 SSA was shown in the afternoon, which was mainly related to the reduction of absorbing
361 aerosols emission, and more secondary scattering aerosol produced by strong chemical
362 reactions under intensive solar radiation and high temperature in the afternoon (Han et al.,
363 2017).

364 **3.2 Aerosol radiative effect**

365 To study the climate impact of the aerosol particles, we investigated the variation of
366 aerosol radiative forcing efficiency (RFE) at the top-of-the-atmosphere (TOA) variations.
367 As seen in Fig. 4, RFE for PM_{10} and PM_1 were always negative during the whole
368 observation period, suggesting that the aerosols measured in urban Beijing have a stable
369 cooling effect on the climate. RFE for PM_{10} and PM_1 at dry condition were -27.0 and $-$
370 $26.2 \text{ W m}^{-2} \text{ AOD}^{-1}$ in 2021 in urban Beijing, which was slightly negative than that of -24.9
371 $\text{W m}^{-2} \text{ AOD}^{-1}$ in Nanjing (Shen et al., 2018) and highly negative than that of -19.9 W m^{-2}
372 AOD^{-1} in Finland (Virkkula et al., 2011). This suggested that the aerosols in urban Beijing
373 have a higher cooling efficiency. ~~RFE was affected by SSA and backscattering ratio~~In eq.

374 (6) The fractional day length (D), solar constant (S_0), atmospheric transmission (T_{at}),
375 fractional cloud amount (A_c), and surface reflectance (R_s) were constants, which were
376 widely used in previous studies (Delene and Ogren, 2002; Andrews et al., 2011; Sherman
377 et al., 2015; Shen et al., 2018). These values are the globally averaged values and don't
378 always represent the conditions in Beijing, but using the same constants makes it possible
379 to compare the intrinsic forcing efficiency of the aerosols measured at different stations
380 around the world and to study how the RFE changes with varying SSA and b (Sherman et
381 al., 2015; Luoma et al., 2019). On the other hand, RFE is sensitive to RH as the aerosol
382 optical properties are different due to hygroscopic growth (Fierz-Schmidhauser et al., 2010;
383 Luoma et al., 2019). Previous studies demonstrate that SSA increases with RH, while b
384 decreases with increasing RH (Carrico et al., 2003; Cheng et al., 2008). The change of SSA
385 to increase with RH and of b to decrease with RH will have opposite effects on the RFE,
386 and thus to some extent, the RH dependencies of these two parameters will counterbalance
387 each other (Luoma et al., 2019). Titos et al. (2021) found that the range of forcing
388 enhancement in different types of sites varies from almost no enhancement up to a factor
389 of 3–4 at RH=90 %. The results observed in urban Beijing showed that the aerosol radiative
390 forcing at RH = 80 % was 1.48 times that under dry conditions (Xia et al., 2023). RFE was
391 calculated at a dry state in this study, while the atmosphere is not generally dry in the
392 ambient air. Thus, the RFE in this study does not represent ambient conditions. The
393 simplified RFE in this study does not represent the actual value for the aerosol forcing;
394 however, it can still indicate how the changes in aerosol optical properties affect the climate
395 (Delene and Ogren, 2002; Andrews et al., 2011; Sherman et al., 2015). RFE was affected
396 by SSA and backscatter fraction (b) and we investigated the RFE variations with SSA and

397 b in Beijing. As shown in Fig. 5, When SSA increases from 0.7 to 0.92, the mean RFE
398 increases by 1.59 times, suggesting that SSA plays an important role in strengthening
399 cooling efficiency. When SSA>0.92, the mean RFE relatively keeps constant. The
400 approximate constant RFE does not mean that the absolute aerosol radiative forcing is
401 constant; it just suggests that the intrinsic nature of the aerosol will not significantly affect
402 the calculation of RFE (Andrews et al., 2011). Also, the ~~backscattering ratio~~
403 backscatter fraction has a negative relationship with RFE. A lower values of ~~backscattering~~
404 ratio~~backscatter fraction~~ corresponds to larger particles (Luoma et al., 2019). RFE became
405 more negative with increasing b, suggesting that smaller particles would cool the
406 atmosphere more efficiently. During the study period, SSA increased from 0.89 to 0.93,
407 while the yearly mean value of b was 0.13 every year during the study period. RFE became
408 more negative from 2018 to 2021, suggesting that the efficiency of the aerosol cooling
409 atmosphere was higher, which was mainly influenced by increasing SSA.

410 The ratio of $\Delta F/AOD$ is known as the aerosol radiative forcing efficiency (RFE) and
411 ΔF at TOA was calculated by multiplying the RFE for PM_{10} with the AOD of ambient
412 atmospheric aerosols observed at the CAMS site during the study periods. The mean value
413 of ΔF from 2018-2021 was -15.0 W m^{-2} , -12.5 W m^{-2} , -12.1 W m^{-2} , and -11.8 W m^{-2} ,
414 respectively. Although RFE became more negative, the annual mean ΔF in 2021
415 corresponding to lower columnar aerosol loading became less negative than that of 2018
416 corresponding to higher columnar aerosol loading (Fig. S3) which was consistent with the
417 analysis that aerosol loading was a essential factor for the estimation of ΔF (Andrews et al.,
418 2011; Delene and Ogren, 2002).

419 3.3 Transport and its impact on aerosol optical properties in Beijing

420 ~~In order to explore the influence of regional transports and the potential source regions~~
421 ~~of pollutants, we analyzed the air mass back trajectories. The~~In addition to local emissions,
422 regional transport is also an important source of particulate matter in Beijing (Chang et al.,
423 2019). Based on previous studies, aerosol source regions and air mass pathways could also
424 affect aerosol optical properties, and the different origins of air masses showed different
425 aerosol optical properties (Zhuang et al., 2015; Pu et al., 2015). The air mass back-
426 trajectories analysis in the North China Plain revealed that the absorption coefficients and
427 SSA were high when the air masses came from densely populated and highly industrial
428 areas (Yan et al., 2008). Therefore, air mass back-trajectories were analyzed in this study
429 to explore the regional transports' influence on aerosol optical properties. First, the air mass
430 back trajectories during 2018–2021 were calculated and clustered (Fig. 7); then, we statistic
431 the aerosol optical properties of each cluster from 2018-2021 (Fig. 8). Based on the
432 Euclidean distance, the back trajectories were classified into five clusters, in which clusters
433 1, 2 and 3, which originated from the clean areas in Mongolia and eastern Inner Mongolia,
434 and transported to Beijing along the pathway with low emissions, were corresponded to
435 low σ_{ab} and low $PM_{2.5}$ (Fig. 8a, d). Cluster 4 from the south of Beijing and cluster 5 from
436 the west of Beijing were referred to as the polluted air masses, and the average $PM_{2.5}$
437 concentrations and σ_{ab} of clusters 4 and 5 were higher than those of clusters 1, 2, and 3 in
438 each year (Fig. 8a, d). Cluster 4 passed through Shandong and Hebei Province, which was
439 heavily polluted before arriving in Beijing. Cluster 5 passed through polluted Shanxi and
440 Hebei during transport. Higher σ_{ab} and $PM_{2.5}$ mass concentrations were mainly distributed
441 in clusters 4 and 5 each year. Lower AAE in cluster 4 indicates that the southern air mass

442 carries more freshly emitted BC particles. SSA of cluster 4 from the south was higher (Fig.
443 8b), which may relate to low BC/PM_{2.5} ratios in south air masses (Xia et al., 2020). Zhang
444 et al. (2013) found that high levels of secondary inorganic aerosols related to high humidity
445 were transported by southern air masses, which enhanced heterogeneous reaction and
446 led to relatively low BC/PM_{2.5} ratios. Fig. 7b showed percentage of each cluster
447 accounting for the total back trajectories in each year. The results indicated that variation
448 in each cluster fraction from 2018 to 2021 was slight. In general, cluster 1-5 accounted for
449 19%-21%, 13%-17%, 16%-20%, 29%-36%, 12%-20% of total back trajectories,
450 respectively. Notably, the percentage of polluted-relevant air masses (cluster 4 and cluster
451 5) was ~50% each year, indicating that the transport from the south and the west of has a
452 considerable impact on the aerosol optical properties. ~~Higher σ_{ab} and PM_{2.5} mass~~
453 ~~concentrations were mainly distributed in clusters 4 and 5 in each year. σ_{ab} and PM_{2.5}~~
454 corresponding to clusters 4 and 5 decreased evidently by 47.3% and 58.4%, and a decrease
455 of PM_{2.5} mass concentration from clusters 4 and 5 was 38.9% and 37.4% during 2018 to
456 2021 (Fig. 8a, d), which may result from the air quality has improved caused by control of
457 source emissions in surrounding regions of Beijing. Therefore, the comprehensive control
458 of atmospheric pollution in Beijing and surrounding regions would be highly effective in
459 reducing air pollution in Beijing.

460 **4 Conclusions**

461 In this study, 4-year measurements of aerosol absorption properties and single
462 scattering albedo for PM₁₀ and PM₁ in Beijing were analyzed. The annual mean PM_{2.5} in
463 2018 was 54.7 $\mu\text{g m}^{-3}$, and it decreased by 34.4% (35.9 $\mu\text{g m}^{-3}$) in 2021, which suggested

464 that the strict pollution control measures are effective in reducing the PM loadings in
465 Beijing. The annual mean σ_{ab} of PM₁₀ and PM₁ decreased by 55.0% and 53.5%,
466 respectively, and it showed a similar ~~decreasing trend in all seasons.~~ decrease in all seasons.
467 Significant reduction in σ_{ab} may be related to reduced primary emissions caused by
468 effective air pollution control measures. SSA at 550 nm increased from 0.89 ± 0.04 for
469 PM₁₀ (0.87 ± 0.05 for PM₁) in 2018 to 0.93 ± 0.03 for PM₁₀ (0.91 ± 0.04 for PM₁) in 2021
470 and the seasonal averages of SSA for two sizes also increased in four seasons. ~~These results~~
471 ~~imply~~ Increasing SSA and decreasing PM_{2.5} mass concentration suggest that the fraction of
472 absorbing aerosols ~~are effectively controlled~~ decreased with improved air quality due to
473 pollution control measure-taking. ~~On the other hand, increasing SSA also implied that~~
474 ~~scattering aerosols play a more important role in radiative forcing in urban Beijing.~~ During
475 the study period, the annual average of Rab increased year by year and was up to 89.2% in
476 2021, indicating that fine particles are the main contributors to the total PM₁₀ particle
477 absorption, and the contributions from fine particles to absorption became more important
478 in Beijing.

479 During the study period, AAE was lowest in summer and highest in winter. Seasonal
480 mean AAE in summer was generally close to 1 indicating that freshly emitted BC from
481 traffic sources was a major component of light-absorbing aerosols. ~~Highest~~ The highest
482 AAE highlights the importance of BrC light absorption in winter. Notably, AAE in winter
483 decreased from 2018 to 2021, implying a decreasing contribution from BrC to absorption,
484 which may relate to the ~~effect~~ effective control of biomass burning and coal combustion
485 caused by changes in heating energy structure. AAE in spring and autumn was similar,

486 indicating light-absorbing aerosols were from similar emission sources in these two
487 seasons.

488 Using a simple analytical equation, we investigated the aerosol radiative effect.
489 Aerosol radiative forcing efficiency (RFE) for PM_{10} and PM_1 was always negative,
490 suggesting that the aerosols measured in urban Beijing have a stable cooling effect on the
491 climate. RFE for PM_{10} and PM_1 at dry conditions were -27.0 and $-26.2 \text{ W m}^{-2} \text{ AOD}^{-1}$ in
492 2021 in urban Beijing. RFE was influenced by SSA and b . Higher b corresponds to more
493 negative RFE suggesting that smaller particles larger would cool the atmosphere more
494 efficiently. When $SSA < 0.92$, the absolute value of mean RFE increased by 1.59 times,
495 suggesting that SSA plays an important role in strengthening cooling efficiency. When
496 $SSA > 0.92$, the mean RFE keeps relatively constant, suggesting that the intrinsic nature of
497 the aerosol will not significantly affect the calculation of RFE. SSA increased from 0.89 to
498 0.93, while the yearly mean value of b was 0.13 every year during the study period. RFE
499 became more negative from 2018 to 2021, suggesting that the efficiency of the aerosol
500 cooling atmosphere was higher, which was mainly influenced by increasing SSA.

501 Regional transport and its impact on aerosol optical properties were also analyzed.
502 The air mass back trajectories arriving at Beijing were divided into five clusters. Clusters
503 1, 2, and 3, which originated from the clean area in Mongolia and eastern Inner Mongolia,
504 were transported to Beijing along the pathway with low emissions, corresponding to low
505 σ_{ab} and low $PM_{2.5}$. Air masses from south and west (Cluster 4 and Cluster 5), which both
506 crossed the polluted region, always brought high $PM_{2.5}$ concentrations and σ_{ab} . σ_{ab} ~~and~~
507 $PM_{2.5}$ -corresponding to clusters 4 and 5 decreased evidently by 47.3% and 58.4%, and a
508 decrease of $PM_{2.5}$ mass concentration from clusters 4 and 5 was 38.9% and 37.4% during

509 2018 ~~to~~ 2021, which may result from the control of source emissions in surrounding
510 regions of Beijing. Therefore, comprehensive control of atmospheric pollution in
511 surrounding regions of Beijing is conducive to reducing pollution in Beijing.

512 **Data availability.**

513 The data in this study are available at: <https://doi.org/10.5281/zenodo.7466069> (Hu et
514 al., 2022)

515 **Competing interests.**

516 The authors declare that they have no conflict of interest.

517 **Author contributions.**

518 ~~XYH analyzed the~~XH performed data analysis, prepared the figures and wrote the
519 manuscript. JYSJS designed the ~~research~~experiment and outlined the manuscript. ~~XYH~~XH,
520 CX, and JYSJS conducted the measurements. ~~All co-authors~~XS, YZ, QL, ZL, SZ, JW, AY,
521 JL, SL and XZ discussed the results and commented on the manuscript.

522 **Acknowledgments.**

523 This study was supported by the National Natural Science Foundation of China
524 (42090031, 41875147, 42075082, 42175128), Chinese Academy of Meteorological
525 Sciences (2022KJ002, 2022KJ005, 2020KJ001, 2020Z002). It was also supported by the
526 Innovation Team for Haze-fog Observation and Forecasts of MOST.

527 **References**

528 Anderson, T. L., and Ogren, J. A.: Determining Aerosol Radiative Properties Using the TSI
529 3563 Integrating Nephelometer, *Aerosol Sci. Technol.*, 29, 57-69,
530 10.1080/02786829808965551, 1998.

531 [Andrews, E., Ogren, J. A., Bonasoni, P., Marinoni, A., Cuevas, E., Rodríguez, S., Sun, J.](#)
532 [Y., Jaffe, D. A., Fischer, E. V., Baltensperger, U., Weingartner, E., Coen, M. C., Sharma, S.,](#)
533 [Macdonald, A. M., Leitch, W. R., Lin, N. H., Laj, P., Arsov, T., Kalapov, I., Jefferson, A.,](#)
534 [and Sheridan, P.: Climatology of aerosol radiative properties in the free troposphere, *Atmos.*](#)
535 [Res., 102, 365-393, 10.1016/j.atmosres.2011.08.017, 2011.](#)

536 Bergin, M. H., Cass, G. R., Xu, J., Fang, C., Zeng, L. M., Yu, T., Salmon, L. G., Kiang, C.
537 S., Tang, X. Y., Zhang, Y. H., and Chameides, W. L.: Aerosol radiative, physical, and
538 chemical properties in Beijing during June 1999, *J. Geophys. Res.*, 106, 17969-17980,
539 10.1029/2001jd900073, 2001.

540 Bond, T. C., Anderson, T. L., and Campbell, D.: Calibration and Intercomparison of Filter-
541 Based Measurements of Visible Light Absorption by Aerosols, *Aerosol Sci. Technol.*, 30,
542 582-600, 10.1080/027868299304435, 1999.

543 Bond, T. C., and Bergstrom, R. W.: Light Absorption by Carbonaceous Particles: An
544 Investigative Review, *Aerosol Sci. Technol.*, 40, 27-67, 10.1080/02786820500421521,
545 2007.

546 Bond, T. C., Doherty, S. J., Fahey, D. W., Forster, P. M., Berntsen, T., DeAngelo, B. J.,
547 Flanner, M. G., Ghan, S., Kärcher, B., Koch, D., Kinne, S., Kondo, Y., Quinn, P. K., Sarofim,
548 M. C., Schultz, M. G., Schulz, M., Venkataraman, C., Zhang, H., Zhang, S., Bellouin, N.,
549 Guttikunda, S. K., Hopke, P. K., Jacobson, M. Z., Kaiser, J. W., Klimont, Z., Lohmann, U.,

550 Schwarz, J. P., Shindell, D., Storelvmo, T., Warren, S. G., and Zender, C. S.: Bounding the
551 role of black carbon in the climate system: A scientific assessment, *J. Geophys. Res.-*
552 *Atmos.*, 118, 5380-5552, 10.1002/jgrd.50171, 2013.

553 [Carrico, C. M., Rood, P. K. a. M. J., and Bates, P. K. Q. a. T. S.: Mixtures of pollution, dust,](#)
554 [sea salt, and volcanic aerosol during ACE-Asia: Radiative properties as a function of](#)
555 [relative humidity, *J. Geophys. Res.*, 108, 8650, 10.1029/2003jd003405, 2003.](#)

556 [Chang, X., Wang, S., Zhao, B., Xing, J., Liu, X., Wei, L., Song, Y., Wu, W., Cai, S., Zheng,](#)
557 [H., Ding, D., and Zheng, M.: Contributions of inter-city and regional transport to PM2.5](#)
558 [concentrations in the Beijing-Tianjin-Hebei region and its implications on regional joint air](#)
559 [pollution control, *Sci Total Environ*, 660, 1191-1200, 10.1016/j.scitotenv.2018.12.474,](#)
560 [2019.](#)

561 Charlson, R. J., Schwartz, S. E., Hales, J. M., Cess, R. D., Coakley, J. A., Hansen, J. E.,
562 and Hofmann, D. J.: Climate Forcing by Anthropogenic Aerosols, *Science*, 255, 423-430,
563 10.1126/science.255.5043.423, 1992.

564 [Cheng, Y. F., Wiedensohler, A., Eichler, H., Su, H., Gnauk, T., Brüggemann, E., Herrmann,](#)
565 [H., Heintzenberg, J., Slanina, J., and Tuch, T.: Aerosol optical properties and related](#)
566 [chemical apportionment at Xinken in Pearl River Delta of China, *Atmospheric*](#)
567 [*Environment*, 42, 6351-6372, 10.1016/j.atmosenv.2008.02.034, 2008.](#)

568 [Collaud Coen, M., Andrews, E., Asmi, A., Baltensperger, U., Bukowiecki, N., Day, D.,](#)
569 [Fiebig, M., Fjaeraa, A. M., Flentje, H., Hyvärinen, A., Jefferson, A., Jennings, S. G.,](#)
570 [Kouvarakis, G., Lihavainen, H., Lund Myhre, C., Malm, W. C., Mihapopoulos, N., Molenaar,](#)
571 [J. V., amp, apos, Dowd, C., Ogren, J. A., Schichtel, B. A., Sheridan, P., Virkkula, A.,](#)
572 [Weingartner, E., Weller, R., and Laj, P.: Aerosol decadal trends – Part 1: In-situ optical](#)

573 [measurements at GAW and IMPROVE stations, Atmos. Chem. Phys., 13, 869-894,](#)
574 [10.5194/acp-13-869-2013, 2013.](#)

575 [Collaud Coen, M., Andrews, E., Alastuey, A., Arsov, T. P., Backman, J., Brem, B. T.,](#)
576 [Bukowiecki, N., Couret, C., Eleftheriadis, K., Flentje, H., Fiebig, M., Gysel-Beer, M.,](#)
577 [Hand, J. L., Hoffer, A., Hooda, R., Hueglin, C., Joubert, W., Keywood, M., Kim, J. E., Kim,](#)
578 [S.-W., Labuschagne, C., Lin, N.-H., Lin, Y., Lund Myhre, C., Luoma, K., Lyamani, H.,](#)
579 [Marinoni, A., Mayol-Bracero, O. L., Mihalopoulos, N., Pandolfi, M., Prats, N., Prenni, A.](#)
580 [J., Putaud, J.-P., Ries, L., Reisen, F., Sellegri, K., Sharma, S., Sheridan, P., Sherman, J. P.,](#)
581 [Sun, J., Titos, G., Torres, E., Tuch, T., Weller, R., Wiedensohler, A., Zieger, P., and Laj, P.:](#)
582 [Multidecadal trend analysis of in situ aerosol radiative properties around the world,](#)
583 [Atmospheric Chemistry and Physics, 20, 8867-8908, 10.5194/acp-20-8867-2020, 2020.](#)

584 [Dai, M., Zhu, B., Fang, C., Zhou, S., Lu, W., Zhao, D., Ding, D., Pan, C., and Liao, H.:](#)
585 [Long-Term Variation and Source Apportionment of Black Carbon at Mt. Waliguan, China,](#)
586 [Journal of Geophysical Research: Atmospheres, 126, 10.1029/2021jd035273, 2021.](#)

587 [Davies, N. W., Fox, C., Szpek, K., Cotterell, M. I., Taylor, J. W., Allan, J. D., Williams, P.](#)
588 [I., Trembath, J., Haywood, J. M., and Langridge, J. M.: Evaluating biases in filter-based](#)
589 [aerosol absorption measurements using photoacoustic spectroscopy, Atmos. Meas. Tech.,](#)
590 [12, 3417-3434, 10.5194/amt-12-3417-2019, 2019.](#)

591 [Delene, D. J., and Ogren, J. A.: Variability of Aerosol Optical Properties at Four North](#)
592 [American Surface Monitoring Sites, J. Aerosol Sci., 59, 1135-1150, 10.1175/1520-](#)
593 [0469\(2002\)059<1135:VOAOPA>2.0.CO;2, 2002.](#)

594 Draxler, R. R., and Hess, G. D.: An overview of the HYSPLIT_4 modelling system of
595 trajectories, dispersion, and deposition, Aust. Meteor. Mag., 47, 295-308, 1998.

596 Dumka, U. C., Kaskaoutis, D. G., Srivastava, M. K., and Devara, P. C. S.: Scattering and
597 absorption properties of near-surface aerosol over Gangetic–Himalayan region: the role of
598 boundary-layer dynamics and long-range transport, *Atmospheric Chemistry and Physics*,
599 15, 1555-1572, 10.5194/acp-15-1555-2015, 2015.

600 Ealo, M., Alastuey, A., Pérez, N., Ripoll, A., Querol, X., and Pandolfi, M.: Impact of
601 aerosol particle sources on optical properties in urban, regional and remote areas in the
602 north-western Mediterranean, *Atmos. Chem. Phys.*, 18, 1149-1169, 10.5194/acp-18-1149-
603 2018, 2018.

604 [Fierz-Schmidhauser, R., Zieger, P., Gysel, M., Kammermann, L., DeCarlo, P. F.,](#)
605 [Baltensperger, U., and Weingartner, E.: Measured and predicted aerosol light scattering](#)
606 [enhancement factors at the high alpine site Jungfrauoch, *Atmos. Chem. Phys.*, 10, 2319–](#)
607 [2333, 2010.](#)

608 Garland, R. M., Schmid, O., Nowak, A., Achtert, P., Wiedensohler, A., Gunthe, S. S.,
609 Takegawa, N., Kita, K., Kondo, Y., and Hu, M.: Aerosol optical properties observed during
610 Campaign of Air Quality Research in Beijing 2006 (CAREBeijing-2006): Characteristic
611 differences between the inflow and outflow of Beijing city air, *J. Geophys. Res.*, 114,
612 D00G04, 10.1029/2008JD010780, 2009.

613 [Gong, S., Zhang, L., Liu, C., Lu, S., Pan, W., and Zhang, Y.: Multi-scale analysis of the](#)
614 [impacts of meteorology and emissions on PM\(2.5\) and O\(3\) trends at various regions in](#)
615 [China from 2013 to 2020 2. Key weather elements and emissions, *Sci Total Environ*, 824,](#)
616 [153847, 10.1016/j.scitotenv.2022.153847, 2022.](#)

617 Gui, K., Yao, W., Che, H., An, L., Zheng, Y., Li, L., Zhao, H., Zhang, L., Zhong, J., Wang,
618 Y., and Zhang, X.: Record-breaking dust loading during two mega dust storm events over

619 northern China in March 2021: aerosol optical and radiative properties and meteorological
620 drivers, *Atmos. Chem. Phys.*, 22, 7905-7932, 10.5194/acp-22-7905-2022, 2022.

621 Guo, J., Miao, Y., Zhang, Y., Liu, H., Li, Z., Zhang, W., He, J., Lou, M., Yan, Y., Bian, L.,
622 and Zhai, P.: The climatology of planetary boundary layer height in China derived from
623 radiosonde and reanalysis data, *Atmos. Chem. Phys.*, 16, 13309-13319, 10.5194/acp-16-
624 13309-2016, 2016.

625 Han, T., Xu, W., Li, J., Freedman, A., Zhao, J., Wang, Q., Chen, C., Zhang, Y., Wang, Z.,
626 Fu, P., Liu, X., and Sun, Y.: Aerosol optical properties measurements by a CAPS single
627 scattering albedo monitor: Comparisons between summer and winter in Beijing, China, *J.*
628 *Geophys. Res.-Atmos.*, 122, 2513-2526, 10.1002/2016jd025762, 2017.

629 Haywood, J. M., and Shine, K. P.: The effect of anthropogenic sulfate and soot aerosol on
630 the clear sky planetary radiation budget, *Geophys. Res. Lett.*, 22(5), 603-606,
631 10.1029/95GL00075, 1995.

632 He, X., Li, C. C., Lau, A. K. H., Deng, Z. Z., Mao, J. T., Wang, M., and Liu, X., Y.: An
633 intensive study of aerosol optical properties in Beijing urban area, *Atmos. Chem. Phys.*, 9,
634 8903-8915, 10.5194/acp-9-8903-2009, 2009.

635 Helin, A., Virkkula, A., Backman, J., Pirjola, L., Sippula, O., Aakko-Saksa, P., Väätäinen,
636 S., Mylläri, F., Järvinen, A., Bloss, M., Aurela, M., Jakobi, G., Karjalainen, P.,
637 Zimmermann, R., Jokiniemi, J., Saarikoski, S., Tissari, J., Rönkkö, T., Niemi, J. V., and
638 Timonen, H.: Variation of Absorption Ångström Exponent in Aerosols From Different
639 Emission Sources, *J. Geophys. Res.-Atmos.*, 126, 10.1029/2020jd034094, 2021.

640 Hu, X., Sun, J., Xia, C., Shen, X., Zhang, Y., Zhang, X., and Zhang, S.: Simultaneous
641 measurements of PM₁ and PM₁₀ aerosol scattering properties and their relationships in

642 urban Beijing: A two-year observation, *Sci. Total Environ.*, 770, 145215,
643 10.1016/j.scitotenv.2021.145215, 2021.

644 Hu, X., Sun, J., Xia, C., Shen, X., Zhang, Y., Liu, Q., Liu, Z., Zhang, S., Wang, J., Yu, A.,
645 Lu, J., Liu, S., and Zhang, X.: Rapid decline of aerosol absorption coefficient and aerosol
646 optical properties effects on radiative forcing in urban areas of Beijing from 2018 to 2021
647 [Data set], Zenodo, <https://doi.org/10.5281/zenodo.7466069>, 2022.

648 J. Hansen, M. Sato, and Ruedy, R.: Radiative forcing and climate response, *J. Geophys.*
649 *Res.*, 102, 6831-6864, 10.1029/96jd03436, 1997.

650 Jacobson, M. Z.: Strong radiative heating due to the mixing state of black carbon in
651 atmospheric aerosols, *Nature*, 409, 695-697, 10.1038/35055518, 2001.

652 Ji, D., Gao, W., Maenhaut, W., He, J., Wang, Z., Li, J., Du, W., Wang, L., Sun, Y., Xin, J.,
653 Hu, B., and Wang, Y.: Impact of air pollution control measures and regional transport on
654 carbonaceous aerosols in fine particulate matter in urban Beijing, China: insights gained
655 from long-term measurement, *Atmos. Chem. Phys.*, 19, 8569-8590, 10.5194/acp-19-8569-
656 2019, 2019.

657 Ji, D., Li, J., Shen, G., He, J., Gao, W., Tao, J., Liu, Y., Tang, G., Zeng, L., Zhang, R., and
658 Wang, Y.: Environmental effects of China's coal ban policy: Results from in situ
659 observations and model analysis in a typical rural area of the Beijing-Tianjin-Hebei region,
660 China, *Atmos. Res.*, 268, 10.1016/j.atmosres.2022.106015, 2022.

661 [Jia, M., Evangeliou, N., Eckhardt, S., Huang, X., Gao, J., Ding, A., and Stohl, A.: Black](#)
662 [Carbon Emission Reduction Due to COVID-19 Lockdown in China, *Geophys Res Lett*, 48,](#)
663 [e2021GL093243, 10.1029/2021GL093243, 2021.](#)

664 Jing, J., Wu, Y., Tao, J., Che, H., Xia, X., Zhang, X., Yan, P., Zhao, D., and Zhang, L.:

665 Observation and analysis of near-surface atmospheric aerosol optical properties in urban
666 Beijing, *Particuology*, 18, 144-154, 10.1016/j.partic.2014.03.013, 2015.

667 Lack, D. A., and Cappa, C. D.: Impact of brown and clear carbon on light absorption
668 enhancement, single scatter albedo and absorption wavelength dependence of black carbon,
669 *Atmos. Chem. Phys.*, 10, 4207-4220, 10.5194/acp-10-4207-2010, 2010.

670 [Laj, P., Bigi, A., Rose, C., Andrews, E., Lund Myhre, C., Collaud Coen, M., Lin, Y.,](#)
671 [Wiedensohler, A., Schulz, M., Ogren, J. A., Fiebig, M., Gliß, J., Mortier, A., Pandolfi, M.,](#)
672 [Petäjä, T., Kim, S.-W., Aas, W., Putaud, J.-P., Mayol-Bracero, O., Keywood, M., Labrador,](#)
673 [L., Aalto, P., Ahlberg, E., Alados Arboledas, L., Alastuey, A., Andrade, M., Artíñano, B.,](#)
674 [Ausmeel, S., Arsov, T., Asmi, E., Backman, J., Baltensperger, U., Bastian, S., Bath, O.,](#)
675 [Beukes, J. P., Brem, B. T., Bukowiecki, N., Conil, S., Couret, C., Day, D., Dayantolis, W.,](#)
676 [Degorska, A., Eleftheriadis, K., Fetfatzis, P., Favez, O., Flentje, H., Gini, M. I., Gregorič,](#)
677 [A., Gysel-Beer, M., Hallar, A. G., Hand, J., Hoffer, A., Hueglin, C., Hooda, R. K.,](#)
678 [Hyvärinen, A., Kalapov, I., Kalivitis, N., Kasper-Giebl, A., Kim, J. E., Kouvarakis, G.,](#)
679 [Kranjc, I., Krejci, R., Kulmala, M., Labuschagne, C., Lee, H.-J., Lihavainen, H., Lin, N.-](#)
680 [H., Löschau, G., Luoma, K., Marinoni, A., Martins Dos Santos, S., Meinhardt, F., Merkel,](#)
681 [M., Metzger, J.-M., Mihalopoulos, N., Nguyen, N. A., Ondracek, J., Pérez, N., Perrone, M.](#)
682 [R., Petit, J.-E., Picard, D., Pichon, J.-M., Pont, V., Prats, N., Prenni, A., Reisen, F., Romano,](#)
683 [S., Sellegri, K., Sharma, S., Schauer, G., Sheridan, P., Sherman, J. P., Schütze, M., Schwerin,](#)
684 [A., Sohmer, R., Sorribas, M., Steinbacher, M., Sun, J., Titos, G., Toczko, B., Tuch, T., Tulet,](#)
685 [P., Tunved, P., Vakkari, V., Velarde, F., Velasquez, P., Villani, P., Vratolis, S., Wang, S.-H.,](#)
686 [Weinhold, K., Weller, R., Yela, M., Yus-Diez, J., Zdimal, V., Zieger, P., and Zikova, N.: A](#)
687 [global analysis of climate-relevant aerosol properties retrieved from the network of Global](#)

688 [Atmosphere Watch \(GAW\) near-surface observatories, Atmospheric Measurement](#)
689 [Techniques, 13, 4353-4392, 10.5194/amt-13-4353-2020, 2020.](#)

690 [Le, T., Wang, Y., Liu, L., Yang, J., Yung, Y. L., Li, G., and Seinfeld, J. H.: Unexpected air](#)
691 [pollution with marked emission reductions during the COVID-19 outbreak in China,](#)
692 [Science, 369, 702-706, 10.1126/science.abb7431, 2020.](#)

693 Lee, K. H., Li, Z., Wong, M. S., Xin, J., Wang, Y., Hao, W.-M., and Zhao, F.: Aerosol single
694 scattering albedo estimated across China from a combination of ground and satellite
695 measurements, *J. Geophys. Res.*, 112, 10.1029/2007jd009077, 2007.

696 Lei, L., Zhou, W., Chen, C., He, Y., Li, Z., Sun, J., Tang, X., Fu, P., Wang, Z., and Sun, Y.:
697 Long-term characterization of aerosol chemistry in cold season from 2013 to 2020 in
698 Beijing, China, *Environ. Pollut.*, 268, 115952, 10.1016/j.envpol.2020.115952, 2021.

699 Li, J., Carlson, B. E., Yung, Y. L., Lv, D., Hansen, J., Penner, J. E., Liao, H., Ramaswamy,
700 V., Kahn, R. A., Zhang, P., Dubovik, O., Ding, A., Lacis, A. A., Zhang, L., and Dong, Y.:
701 Scattering and absorbing aerosols in the climate system, *Nature Reviews Earth &*
702 *Environment*, 10.1038/s43017-022-00296-7, 2022a.

703 Li, W., Liu, X., Duan, F., Qu, Y., and An, J.: A one-year study on black carbon in urban
704 Beijing: Concentrations, sources and implications on visibility, *Atmos. Pollut. Res.*, 13,
705 10.1016/j.apr.2021.101307, 2022b.

706 Liu, G. J., Xin, J. Y., Wang, X., Si, R. R., Ma, Y. N., Wen, T. X., Zhao, L., Zhao, D. D.,
707 Wang, Y. S., and Gao, W. K.: Impact of the coal banning zone on visibility in the Beijing-
708 Tianjin-Hebei region, *Sci. Total Environ.*, 692, 402-410, 10.1016/j.scitotenv.2019.07.006,
709 2019.

710 [Liu, Y., Wang, Y., Cao, Y., Yang, X., Zhang, T., Luan, M., Lyu, D., Hansen, A. D. A., Liu,](#)

711 [B., and Zheng, M.: Impacts of COVID-19 on Black Carbon in Two Representative Regions](#)
712 [in China: Insights Based on Online Measurement in Beijing and Tibet, Geophysical](#)
713 [Research Letters, 48, 10.1029/2021gl092770, 2021.](#)

714 Luo, L., Tian, H., Liu, H., Bai, X., Liu, W., Liu, S., Wu, B., Lin, S., Zhao, S., Hao, Y., Sun,
715 Y., Hao, J., and Zhang, K.: Seasonal variations in the mass characteristics and optical
716 properties of carbonaceous constituents of PM_{2.5} in six cities of North China, Environ.
717 Pollut., 268, 115780, 10.1016/j.envpol.2020.115780, 2020.

718 [Luoma, K., Virkkula, A., Aalto, P., Petäjä, T., and Kulmala, M.: Over a 10-year record of](#)
719 [aerosol optical properties at SMEAR II, Atmos. Chem. Phys., 19, 11363-11382,](#)
720 [10.5194/acp-19-11363-2019, 2019.](#)

721 Moosmüller, H., Chakrabarty, R. K., and Arnott, W. P.: Aerosol light absorption and its
722 measurement: A review, J. Quant. Spectrosc. Radiat. Transf., 110, 844-878,
723 10.1016/j.jqsrt.2009.02.035, 2009.

724 Ogren, J. A., Wendell, J., Andrews, E., and Sheridan, P. J.: Continuous light absorption
725 photometer for long-term studies, Atmos. Meas. Tech., 10, 4805-4818, 10.5194/amt-10-
726 4805-2017, 2017.

727 [Pandolfi, M., Alados-Arboledas, L., Alastuey, A., Andrade, M., Angelov, C., Artiñano, B.,](#)
728 [Backman, J., Baltensperger, U., Bonasoni, P., Bukowiecki, N., Collaud Coen, M., Conil,](#)
729 [S., Coz, E., Crenn, V., Dudoitis, V., Ealo, M., Eleftheriadis, K., Favez, O., Fetfatzis, P.,](#)
730 [Fiebig, M., Flentje, H., Ginot, P., Gysel, M., Henzing, B., Hoffer, A., Holubova Smejkalova,](#)
731 [A., Kalapov, I., Kalivitis, N., Kouvarakis, G., Kristensson, A., Kulmala, M., Lihavainen,](#)
732 [H., Lunder, C., Luoma, K., Lyamani, H., Marinoni, A., Mihalopoulos, N., Moerman, M.,](#)
733 [Nicolas, J., amp, apos, Dowd, C., Petäjä, T., Petit, J.-E., Pichon, J. M., Prokopciuk, N.,](#)

734 [Putaud, J.-P., Rodríguez, S., Sciare, J., Sellegri, K., Swietlicki, E., Titos, G., Tuch, T.,](#)
735 [Tunved, P., Ulevicius, V., Vaishya, A., Vana, M., Virkkula, A., Vratolis, S., Weingartner, E.,](#)
736 [Wiedensohler, A., and Laj, P.: A European aerosol phenomenology – 6: scattering](#)
737 [properties of atmospheric aerosol particles from 28 ACTRIS sites, Atmospheric Chemistry](#)
738 [and Physics, 18, 7877-7911, 10.5194/acp-18-7877-2018, 2018.](#)

739 [Pu, W., Zhao, X., Shi, X., Ma, Z., Zhang, X., and Yu, B.: Impact of long-range transport on](#)
740 [aerosol properties at a regional background station in Northern China, Atmospheric](#)
741 [Research, 153, 489-499, 10.1016/j.atmosres.2014.10.010, 2015.](#)

742 Ran, L., Deng, Z. Z., Wang, P. C., and Xia, X. A.: Black carbon and wavelength-dependent
743 aerosol absorption in the North China Plain based on two-year aethalometer measurements,
744 Atmos. Environ., 142, 132-144, 10.1016/j.atmosenv.2016.07.014, 2016.

745 Segura, S., Estellés, V., Esteve, A. R., Marcos, C. R., Utrillas, M. P., and Martínez-Lozano,
746 J. A.: Multiyear in-situ measurements of atmospheric aerosol absorption properties at an
747 urban coastal site in western Mediterranean, Atmos. Environ., 129, 18-26,
748 10.1016/j.atmosenv.2016.01.008, 2016.

749 [Shen, Y., Virkkula, A., Ding, A., Wang, J., Chi, X., Nie, W., Qi, X., Huang, X., Liu, Q.,](#)
750 [Zheng, L., Xu, Z., Petäjä, T., Aalto, P. P., Fu, C., and Kulmala, M.: Aerosol optical](#)
751 [properties at SORPES in Nanjing, east China, Atmos. Chem. Phys., 18, 5265-5292,](#)
752 [10.5194/acp-18-5265-2018, 2018.](#)

753 [Sheridan, P. J., and Ogren, J. A.: Observations of the vertical and regional variability of](#)
754 [aerosol optical properties over central and eastern North America, J. Geophys. Res., 104,](#)
755 [16793-16805, 10.1029/1999jd900241, 1999.](#)

756 [Sherman, J. P., Sheridan, P. J., Ogren, J. A., Andrews, E., Hageman, D., Schmeisser, L.,](#)

757 [Jefferson, A., and Sharma, S.: A multi-year study of lower tropospheric aerosol variability](#)
758 [and systematic relationships from four North American regions, Atmospheric Chemistry](#)
759 [and Physics, 15, 12487-12517, 10.5194/acp-15-12487-2015, 2015.](#)

760 Sun, J., Wang, Z., Zhou, W., Xie, C., Wu, C., Chen, C., Han, T., Wang, Q., Li, Z., Li, J., Fu,
761 P., Wang, Z., and Sun, Y.: Measurement report: Long-term changes in black carbon and
762 aerosol optical properties from 2012 to 2020 in Beijing, China, Atmos. Chem. Phys., 22,
763 561-575, 10.5194/acp-22-561-2022, 2022.

764 Sun, Y., Xu, W., Zhang, Q., Jiang, Q., Canonaco, F., Prévôt, A. S. H., Fu, P., Li, J., Jayne,
765 J., Worsnop, D. R., and Wang, Z.: Source apportionment of organic aerosol from 2-year
766 highly time-resolved measurements by an aerosol chemical speciation monitor in Beijing,
767 China, Atmos. Chem. Phys., 18, 8469-8489, 10.5194/acp-18-8469-2018, 2018.

768 Sun, Y., Lei, L., Zhou, W., Chen, C., He, Y., Sun, J., Li, Z., Xu, W., Wang, Q., Ji, D., Fu, P.,
769 Wang, Z., and Worsnop, D. R.: A chemical cocktail during the COVID-19 outbreak in
770 Beijing, China: Insights from six-year aerosol particle composition measurements during
771 the Chinese New Year holiday, Sci Total Environ, 742, 140739,
772 10.1016/j.scitotenv.2020.140739, 2020.

773 Szopa, S., Naik, V., Adhikary, B., Artaxo, P., Berntsen, T., Collins, W. D., Fuzzi, S.,
774 Gallardo, L., Kiendler-Scharr, A., Klimont, Z., Liao, H., Unger, N., and Zanis, P.: Short-
775 Lived Climate Forcers. In Climate Change 2021: The Physical Science Basis. Contribution
776 of Working Group I to the Sixth Assessment Report of the Intergovernmental Panel on
777 Climate Change [Masson-Delmotte, V., P. Zhai, A. Pirani, S.L. Connors, C. Péan, S. Berger,
778 N. Caud, Y. Chen, L. Goldfarb, M.I. Gomis, M. Huang, K. Leitzell, E. Lonnoy, J.B.R.
779 Matthews, T.K. Maycock, T. Waterfield, O. Yelekçi, R. Yu, and B. Zhou (eds.)], Cambridge

780 University Press, Cambridge, United Kingdom and New York, NY, USA, 817-922,
781 10.1017/9781009157896.008, 2021.

782 [Tian, H., Liu, Y., Li, Y., Wu, C. H., Chen, B., Kraemer, M. U. G., Li, B., Cai, J., Xu, B.,](#)
783 [Yang, Q., Wang, B., Yang, P., Cui, Y., Song, Y., Zheng, P., Wang, Q., Bjornstad, O. N., Yang,](#)
784 [R., Grenfell, B. T., Pybus, O. G., and Dye, C.: An investigation of transmission control](#)
785 [measures during the first 50 days of the COVID-19 epidemic in China, Science, 368, 638-](#)
786 [642, 10.1126/science.abb6105, 2020.](#)

787 [Titos, G., Foyo-Moreno, I., Lyamani, H., Querol, X., Alastuey, A., and Alados-Arboledas,](#)
788 [L.: Optical properties and chemical composition of aerosol particles at an urban location:](#)
789 [An estimation of the aerosol mass scattering and absorption efficiencies, Journal of](#)
790 [Geophysical Research, 117, D04206, 10.1029/2011jd016671, 2012.](#)

791 [Titos, G., Burgos, M. A., Zieger, P., Alados-Arboledas, L., Baltensperger, U., Jefferson, A.,](#)
792 [Sherman, J., Weingartner, E., Henzing, B., Luoma, K., O'Dowd, C., Wiedensohler, A., and](#)
793 [Andrews, E.: A global study of hygroscopicity-driven light-scattering enhancement in the](#)
794 [context of other in situ aerosol optical properties, Atmospheric Chemistry and Physics, 21,](#)
795 [13031-13050, 10.5194/acp-21-13031-2021, 2021.](#)

796 Tuch, T. M., Haudek, A., Müller, T., Nowak, A., Wex, H., and Wiedensohler, A.: Design
797 and performance of an automatic regenerating adsorption aerosol dryer for continuous
798 operation at monitoring sites, Atmos. Meas. Tech., 2, 417-422, 10.5194/amt-2-417-2009,
799 2009.

800 Twomey, S.: Pollution and the Planetary Albedo, Atmos. Environ., 41, 120-125,
801 10.1016/j.atmosenv.2007.10.062, 2007.

802 Virkkula, A., Backman, J., Aalto, P. P., Hulkkonen, M., Riuttanen, L., Nieminen, T., dal

803 Maso, M., Sogacheva, L., de Leeuw, G., and Kulmala, M.: Seasonal cycle, size
804 dependencies, and source analyses of aerosol optical properties at the SMEAR II
805 measurement station in Hyytiälä, Finland, *Atmos. Chem. Phys.*, 11, 4445-4468,
806 10.5194/acp-11-4445-2011, 2011.

807 Vu, T. V., Shi, Z., Cheng, J., Zhang, Q., He, K., Wang, S., and Harrison, R. M.: Assessing
808 the impact of clean air action on air quality trends in Beijing using a machine learning
809 technique, *Atmospheric Chemistry and Physics*, 19, 11303-11314, 10.5194/acp-19-11303-
810 2019, 2019.

811 Wang, Q. L., Wang, L. L., Gong, C. S., Li, M. G., Xin, J. Y., Tang, G. Q., Sun, Y., Gao, J.
812 H., Wang, Y. H., Wu, S., Kang, Y. Y., Yang, Y., Li, T. T., Liu, J. D., and Wang, Y. S.: Vertical
813 evolution of black and brown carbon during pollution events over North China Plain, *Sci.*
814 *Total Environ.*, 806, 10.1016/j.scitotenv.2021.150950, 2022.

815 Wang, T., Du, Z., Tan, T., Xu, N., Hu, M., Hu, J., and Guo, S.: Measurement of aerosol
816 optical properties and their potential source origin in urban Beijing from 2013-2017, *Atmos.*
817 *Environ.*, 206, 293-302, 10.1016/j.atmosenv.2019.02.049, 2019.

818 Wang, Y. Q., Zhang, X. Y., and Draxler, R. R.: TrajStat: GIS-based software that uses
819 various trajectory statistical analysis methods to identify potential sources from long-term
820 air pollution measurement data, *Environ. Model Softw.*, 24, 938-939,
821 10.1016/j.envsoft.2009.01.004, 2009.

822 WMO/GAW: WMO/GAW Aerosol Measurement Procedures, Guidelines and
823 Recommendations, Geneva, Switzerland, 2016.

824 Xia, C., Sun, J., Qi, X., Shen, X., Zhong, J., Zhang, X., Wang, Y., Zhang, Y., and Hu, X.:
825 Observational study of aerosol hygroscopic growth on scattering coefficient in Beijing: A

826 case study in March of 2018, *Sci. Total Environ.*, 685, 239-247,
827 10.1016/j.scitotenv.2019.05.283, 2019.

828 [Xia, C., Sun, J., Hu, X., Shen, X., Zhang, Y., Zhang, S., Wang, J., Liu, Q., Lu, J., Liu, S.,](#)
829 [and Zhang, X.: Effects of hygroscopicity on aerosol optical properties and direct radiative](#)
830 [forcing in Beijing: Based on two-year observations, *Sci Total Environ*, 857, 159233,](#)
831 [10.1016/j.scitotenv.2022.159233, 2023.](#)

832 Xia, Y., Wu, Y., Huang, R. J., Xia, X., Tang, J., Wang, M., Li, J., Wang, C., Zhou, C., and
833 Zhang, R.: Variation in black carbon concentration and aerosol optical properties in Beijing:
834 Role of emission control and meteorological transport variability, *Chemosphere*, 254,
835 126849, 10.1016/j.chemosphere.2020.126849, 2020.

836 Xie, C., He, Y., Lei, L., Zhou, W., Liu, J., Wang, Q., Xu, W., Qiu, Y., Zhao, J., Sun, J., Li,
837 L., Li, M., Zhou, Z., Fu, P., Wang, Z., and Sun, Y.: Contrasting mixing state of black carbon-
838 containing particles in summer and winter in Beijing, *Environ. Pollut.*, 263, 114455,
839 10.1016/j.envpol.2020.114455, 2020.

840 Xu, X., and Zhang, T.: Spatial-temporal variability of PM_{2.5} air quality in Beijing, China
841 during 2013-2018, *J. Environ. Manag.*, 262, 110263, 10.1016/j.jenvman.2020.110263,
842 2020.

843 [Yan, P., Tang, J., Huang, J., Mao, J. T., Zhou, X. J., Liu, Q., Wang, Z. F., and Zhou, H. G.:](#)
844 [The measurement of aerosol optical properties at a rural site in Northern China,](#)
845 [*Atmospheric Chemistry and Physics*, 8, 2229–2242, 10.5194/acp-8-2229-2008, 2008.](#)

846 [Yang, M., Howell, S. G., Zhuang, J., and Huebert, B. J.: Attribution of aerosol light](#)
847 [absorption to black carbon, brown carbon, and dust in China – interpretations of](#)
848 [atmospheric measurements during EAST-AIRE, *Atmos. Chem. Phys.*, 9, 2035–2050, 2009.](#)

849 Yi, Z., Wang, Y., Chen, W., Guo, B., Zhang, B., Che, H., and Zhang, X.: Classification of
850 the Circulation Patterns Related to Strong Dust Weather in China Using a Combination of
851 the Lamb–Jenkinson and k-Means Clustering Methods, *Atmosphere*, 12,
852 10.3390/atmos12121545, 2021.

853 Zhang, Q., Zheng, Y., Tong, D., Shao, M., Wang, S., Zhang, Y., Xu, X., Wang, J., He, H.,
854 Liu, W., Ding, Y., Lei, Y., Li, J., Wang, Z., Zhang, X., Wang, Y., Cheng, J., Liu, Y., Shi, Q.,
855 Yan, L., Geng, G., Hong, C., Li, M., Liu, F., Zheng, B., Cao, J., Ding, A., Gao, J., Fu, Q.,
856 Huo, J., Liu, B., Liu, Z., Yang, F., He, K., and Hao, J.: Drivers of improved PM_{2.5} air
857 quality in China from 2013 to 2017, *P. Natl. Acad. Sci. USA*, 116, 24463-24469,
858 10.1073/pnas.1907956116, 2019.

859 [Zhang, R., Jing, J., Tao, J., Hsu, S. C., Wang, G., Cao, J., Lee, C. S. L., Zhu, L., Chen, Z.,](#)
860 [Zhao, Y., and Shen, Z.: Chemical characterization and source apportionment of PM_{2.5} in](#)
861 [Beijing: seasonal perspective, *Atmos. Chem. Phys.*, 13, 7053-7074, 10.5194/acp-13-7053-](#)
862 [2013, 2013.](#)

863 Zhang, Y. Z., Zhi, G. R., Jin, W. J., Wang, L., Guo, S. C., Shi, R., Sun, J. Z., Cheng, M. M.,
864 Bi, F., Gao, J., Zhang, B. J., Wu, J. J., Shi, Z. H., Liu, B., Wang, Z., and Li, S. Y.: Differing
865 effects of escalating pollution on absorption and scattering efficiencies of aerosols: Toward
866 co-beneficial air quality enhancement and climate protection measures, *Atmos. Environ.*,
867 232, 10.1016/j.atmosenv.2020.117570, 2020.

868 Zhao, S. M., Hu, B., Du, C. J., Tang, L. Q., Ma, Y. J., Liu, H., Zou, J. N., Liu, Z. R., Wei,
869 J., and Wang, Y. S.: Aerosol optical characteristics and radiative forcing in urban Beijing,
870 *Atmos. Environ.*, 212, 41-53, 10.1016/j.atmosenv.2019.05.034, 2019.

871 Zhao, S. M., Hu, B., Gao, W. K., Li, L. C., Huang, W., Wang, L. L., Yang, Y., Liu, J. D., Li,

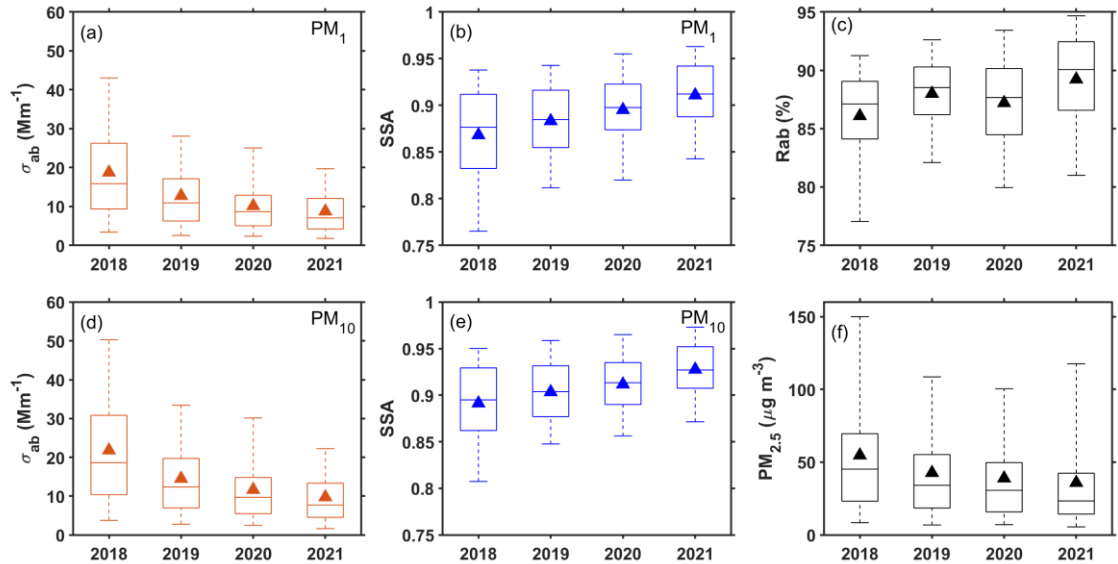
872 J. Y., Ji, D. S., Zhang, R. J., Zhang, Y. Y., and Wang, Y. S.: Effect of the "coal to gas" project
873 on atmospheric NOX during the heating period at a suburban site between Beijing and
874 Tianjin, Atmos. Res., 241, 10.1016/j.atmosres.2020.104977, 2020.

875 [Zhuang, B. L., Wang, T. J., Liu, J., Ma, Y., Yin, C. Q., Li, S., Xie, M., Han, Y., Zhu, J. L.,](#)
876 [Yang, X. Q., and Fu, C. B.: Absorption coefficient of urban aerosol in Nanjing, west](#)
877 [Yangtze River Delta, China, Atmos. Chem. Phys., 15, 13633-13646, 10.5194/acp-15-](#)
878 [13633-2015, 2015.](#)

879

880

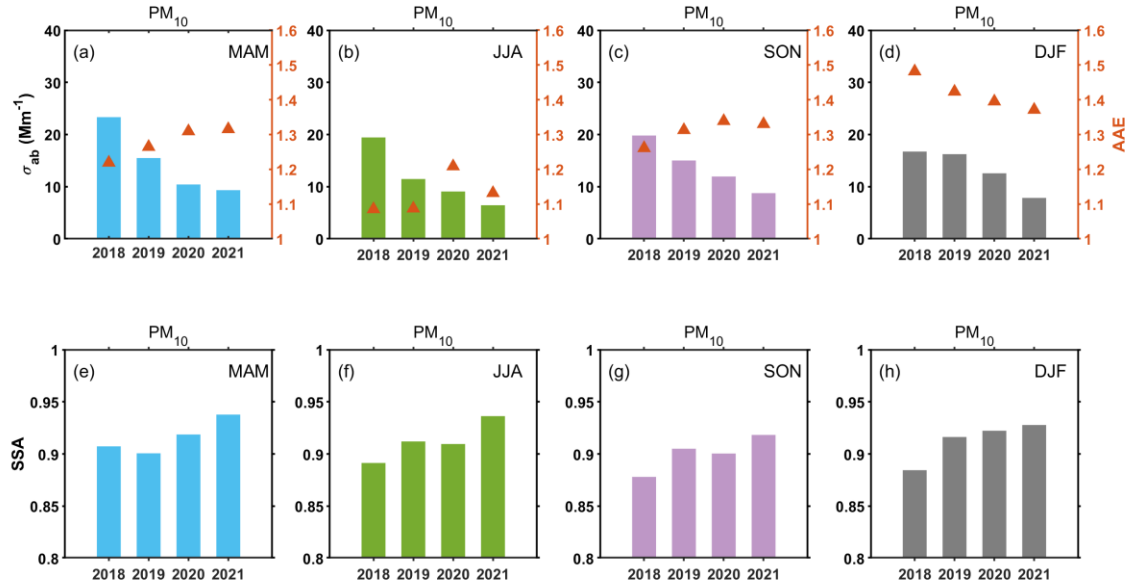
881



882

883 **Figure 1.** Annual variation of aerosol optical properties and $PM_{2.5}$ mass concentration,
884 absorption coefficient σ_{ab} at 550 nm for (a) PM_1 and (d) PM_{10} , SSA at 550 nm for (b) PM_1
885 and (e) PM_{10} , (c) R_{ab} and (f) $PM_{2.5}$ mass concentration. The solid line inside the box
886 represents the median and the triangle indicates the mean. The box contains the range of
887 values from 25% (bottom) to 75% (top), and the upper and lower whiskers are the 95th and
888 5th percentiles, respectively.

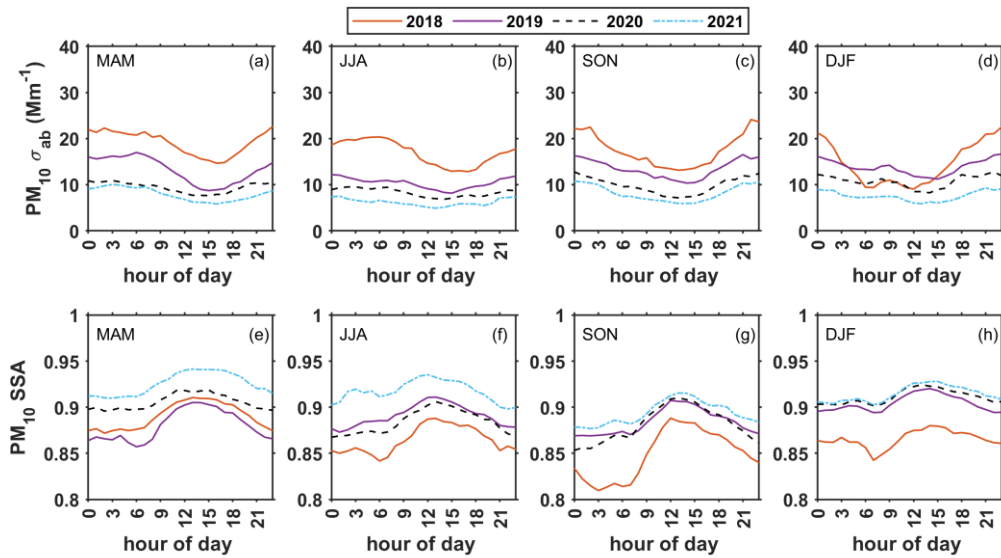
889



890

891 **Figure 2.** Seasonal variation of aerosol optical properties of PM₁₀ from 2018-2021, (a-d)

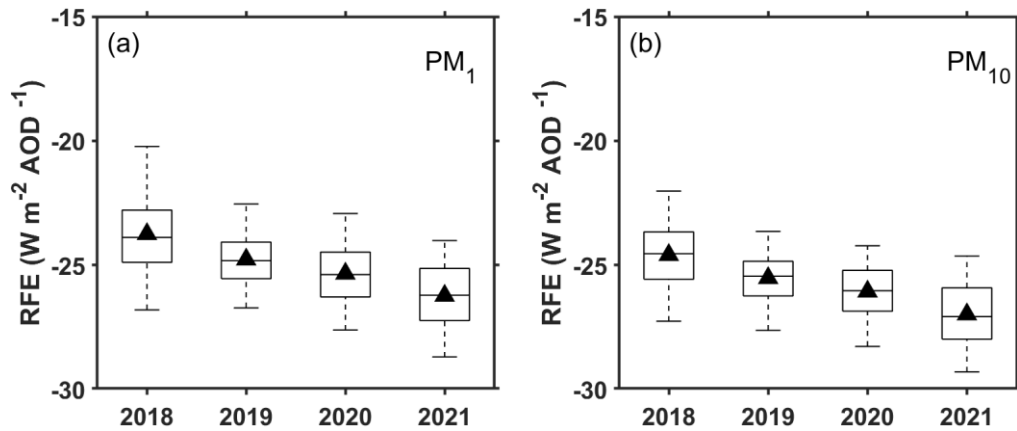
892 σ_{ab} (bar) at 550 nm, $AAE_{450/700}$ (triangle), and (e-h) SSA (bar) at 550 nm.



893

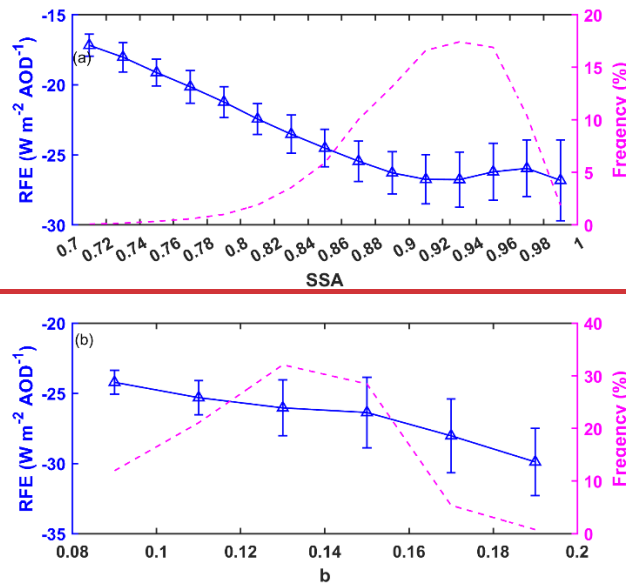
894 **Figure 3.** Diurnal variations of σ_{ab} (a-d) and SSA (e-h) at 550 nm for PM₁₀ in four seasons

895 from 2018 to 2021.

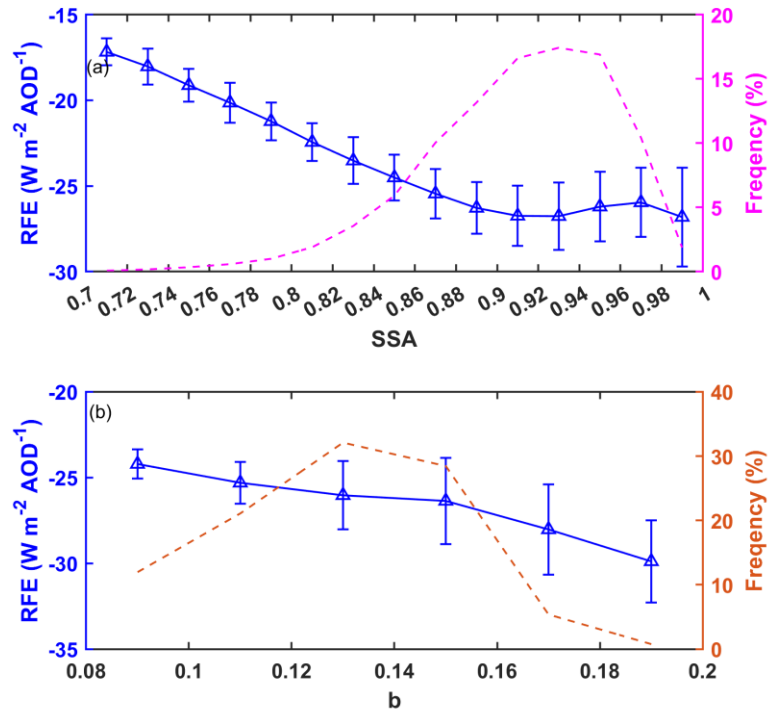


896

897 **Figure 4.** The annual variation of aerosol radiative forcing efficiency for PM_{10} (a) and PM_{1}
 898 (b). The solid line inside the box represents the median, and the triangle indicates the mean.
 899 The box contains the range of values from 25% (bottom) to 75% (top), and the 95th and
 900 5th percentiles, respectively.

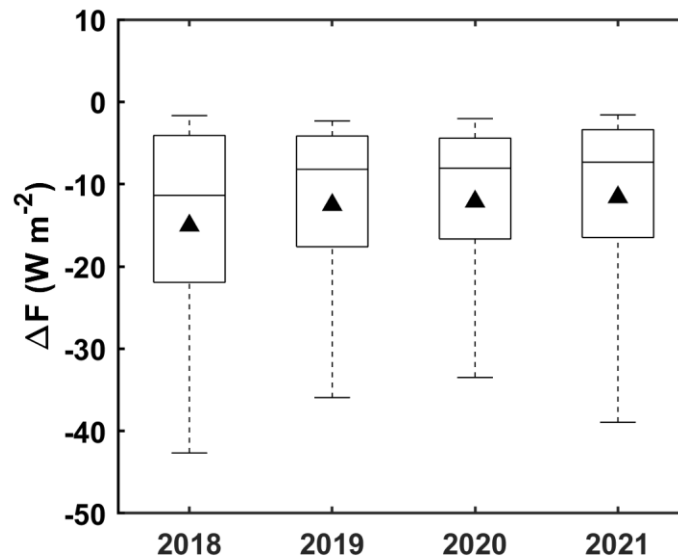


901



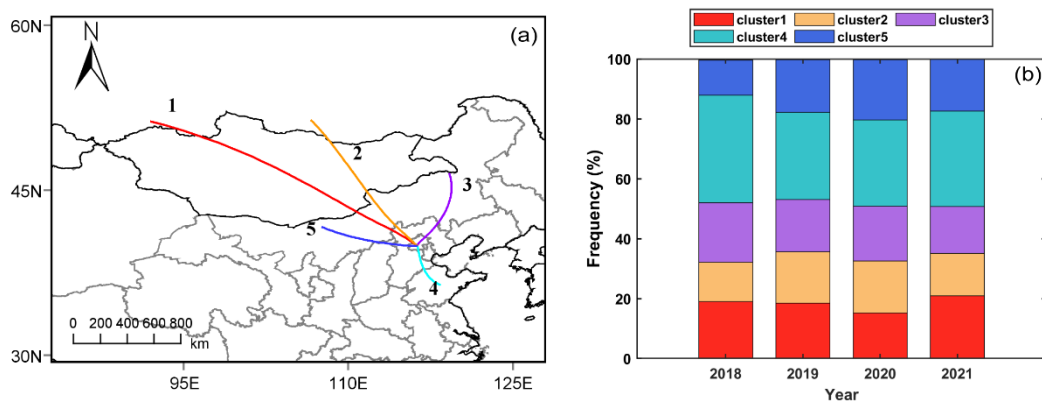
902

903 **Figure 5.** The relationship of RFE with (a) SSA and (b) backscattering ratio:backscatter
 904 fraction. The pink dash line represents the frequency distribution of SSA (a) and
 905 backscattering ratio:the brown dash line represents the frequency distribution of backscatter
 906 fraction (b).



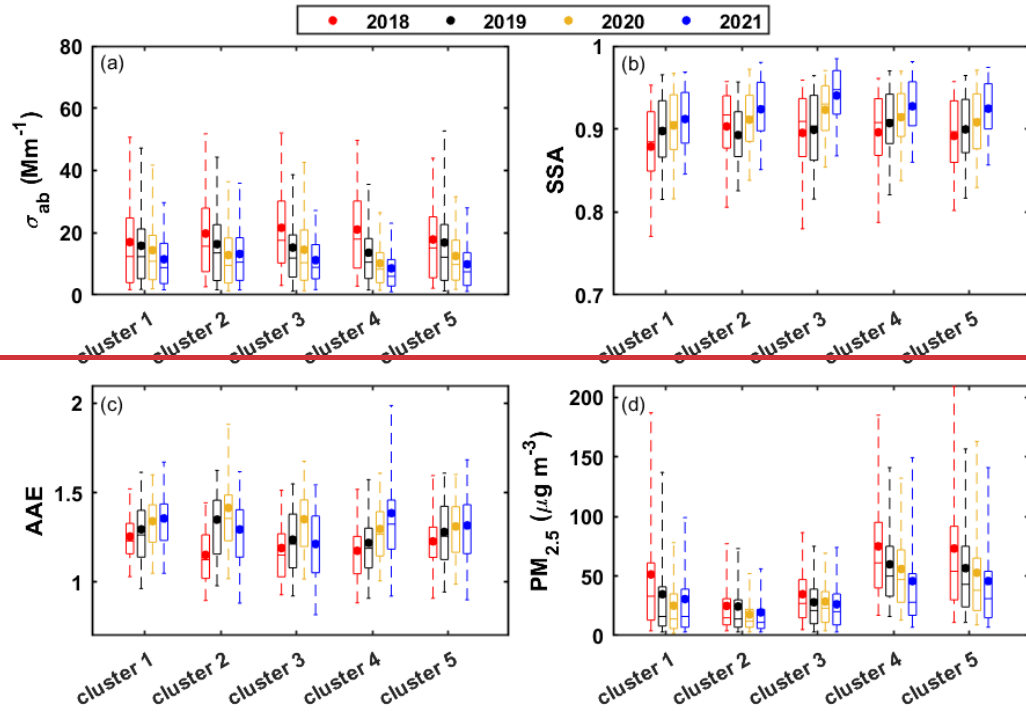
907

908 **Figure 6.** Annual variation of aerosol radiative forcing (ΔF) at TOA from 2018 to 2021
 909 calculated from daily mean data. The solid line inside the box represents the median, and
 910 the triangle indicates the mean. The box contains the range of values from 25% (bottom)
 911 to 75% (top), and the 95th and 5th percentiles, respectively.



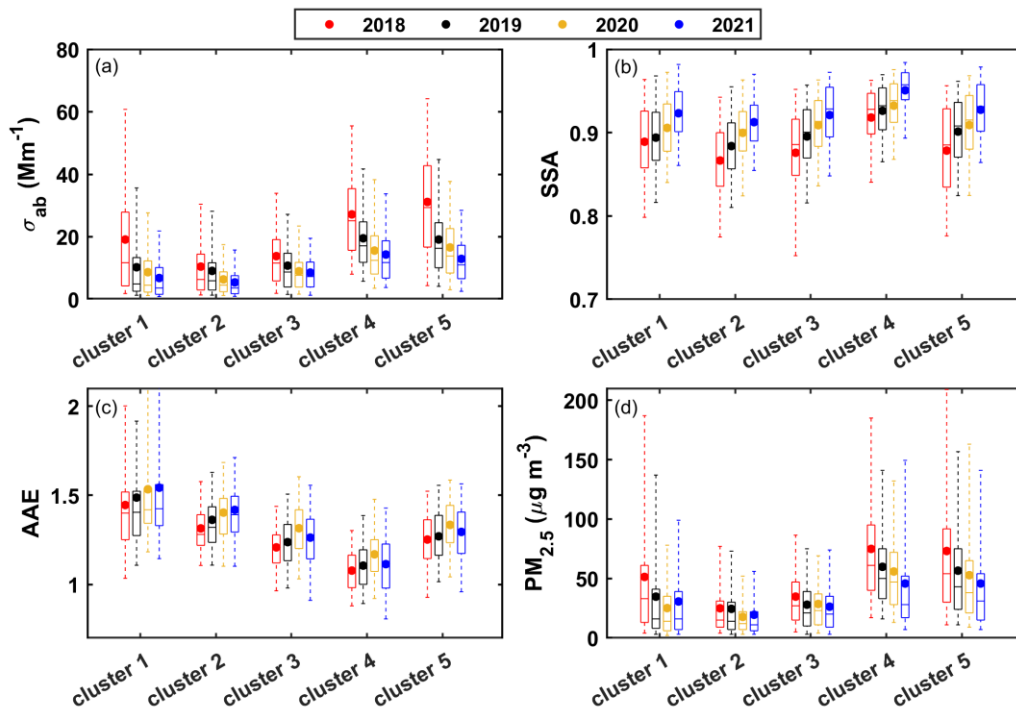
912

913 **Figure 7.** (a) Air mass clusters of back trajectories arriving in Beijing during 2018–2021
 914 and (b) the fraction of each cluster accounting for the total back trajectories in each year.



915

916



917

918 **Figure 8.** The variation of (a) σ_{ab} , (b) SSA, (c) AAE, and $PM_{2.5}$ mass concentration in each
919 cluster from 2018 to 2021. The solid line inside the box represents the median and the dot
920 indicates the mean. The box contains the range of values from 25% (bottom) to 75% (top),
921 and the 95th and 5th percentiles, respectively.
922